# An unloading foam model to constrain Etna's 11-13 January 2011 lava fountaining episode

Calvari S. [1], Salerno G.G. [1], Spampinato L. [1], Gouhier M. [2], La Spina A. [1], Pecora E. [1], Harris A.J.L. [2], Labazuy P. [2], Biale E. [1], and Boschi E. [1]

1 – Istituto Nazionale di Geofisica e Vulcanologia, Osservatorio Etneo, sezione di Catania, Piazza Roma 2, 95125 Catania, Italy

2 – Laboratoire Magmas et Volcans, Université Blaise Pascal, 5 Rue Kessler, 63038 Clermont Ferrand, France

*Corresponding author:*

Sonia Calvari

Istituto Nazionale di Geofisica e Vulcanologia

Osservatorio Etneo, sezione di Catania

Piazza Roma 2

95125 Catania (Italy)

Email: sonia.calvari@ct.ingv.it

Tel: + 39 095 7165862

Fax: + 39 095 716 5826

## Abstract

The 11-13 January 2011 eruptive episode at Etna volcano occurred after several months of increasing ash emissions from the summit craters, and was heralded by increasing $SO_2$ output, which peaked at ~5000 Megagrams/day several hours before the start of the eruptive activity. The eruptive episode began with a phase of strombolian activity from a pit crater on the eastern flank of the SE-Crater. Explosions became more intense with time and eventually became transitional between strombolian and fountaining, before moving into a lava fountaining phase. Fountaining was accompanied by lava output from the lower rim of the pit crater. Emplacement of the resulting lava flow field, as well as associated lava fountain- and strombolian-phases, was tracked using a remote sensing network comprising both thermal and visible cameras. Thermal surveys completed once the eruptive episode had ended also allowed us to reconstruct the emplacement of the lava flow field. Using a high temporal resolution geostationary satellite data we were also able to construct a detailed record of the heat flux during the fountain-fed flow phase and its subsequent cooling. The dense rock volume of erupted lava obtained from the satellite data was $1.2 \times 10^6$ $m^3$; this was emplaced over a period of about 6 hours to give a mean output rate of ~55 $m^3$ $s^{-1}$. By comparison, geologic data allowed us to estimate dense rock volumes of ~$0.85 \times 10^6$ $m^3$ for the pyroclastics erupted during the lava fountain phase, and 0.84-1.7 $\times$ $10^6$ $m^3$ for lavas erupted during the effusive phase, resulting in a total erupted dense rock volume of 1.7-2.5 $\times$ $10^6$ $m^3$ and a mean output rate of 78-117 $m^3$ $s^{-1}$. The sequence of events and quantitative results presented here shed light on the shallow feeding system of the volcano.

## 1. Introduction

Explosive basaltic eruptions span weakly explosive, low volume, emissions such as the persistent explosive activity typical of Stromboli volcano [e.g. *Patrick*, 2007; *Patrick et al*., 2007], to more energetic and higher volume lava fountains which feed columns of scoria, bombs and ash, with jets of molten rock, to heights of tens to hundreds meters [e.g. *Swanson et al*., 1979; *Heliker and Mattox*, 1986]. The weakest end member of types of this repeated explosive activity at a basaltic system is gas-pistoning [e.g. *Ferrazzini et al*., 1991; *Johnson et al.,* 2005] and gas puffing [e.g. *Harris and Ripepe*, 2007].

*Parfitt and Wilson* [1995] have suggested that the primary difference between the so-called strombolian and hawaiian events lies in the ability of bubbles to coalesce and grow. They argue that in hawaiian eruptions there is little coalescence due to fast ascent rates, so that eruptive activity is controlled by the exsolution of many small bubbles at the fragmentation surface. In contrast, they propose that Strombolian activity is fed by the bursting of large gas bubbles, or slugs, at the magma free surface, where the slugs can form by coalescence in more slowly ascending magma. This model differs from that of *Vergniolle and Jaupart* [1986], that explains the transition from strombolian and hawaiian activity using a series of conduit flow regimes, which change depending on gas content, bubble size, and magma viscosity. They suggested that, rather than remaining as a homogeneous flow, hawaiian lava fountaining may involve transitions from bubbly flow to annular flow, in which there is a central stream of gas bounded by liquid moving along the conduit walls. *Vergniolle and Jaupart* [1986] also argued that strombolian eruptions involve transitions from bubbly flow to slug flow, in which large bubbles of gas develop and rise through the residual bubble-poor melt. Using a combination of theoretical models and laboratory experiments, *Jaupart and Vergniolle* [1988] also showed that ascending bubbles can form a foam layer at the roof of a magma reservoir. When the foam layer reaches a threshold thickness, the bubbles coalesce and the foam collapses, generating a slug that enters and ascends the conduit to burst at the free surface. After some time, a new foam layer forms,

thickens and collapses to repeat the cycle. Analyses of magmatic gas measurements during lava fountain events at Etna volcano suggest activity is fed by a gas bubble layer that accumulates prior to the event at a depth of about 1.5 km below the erupting crater [*Allard et al*., 2005]; thus supporting a gas-melt separation model rather than a bulk degassing (rise-speed-dependent) model [*Parfitt*, 2004]. This has been confirmed by other recent multidisciplinary data comprising petrochemistry of ejecta, gravimetry, seismicity, ground and deformation measurements [ *Andronico and Corsaro*, 2011; *Bonaccorso et al*., 2011a, 2011b].

Etna's activity recently moved towards more explosive styles of eruption, which have characterised activity especially since 2000 [e.g. *Behncke et al*., 2006; *Andronico and Corsaro*, 2011; *Harris et al*., 2011]. Thus, the need to understand, recognise and predict such explosive activity is becoming increasingly important at this basaltic system. In this paper we present an integration of remote sensing data collected from a ground-based camera network installed on Etna by Istituto Nazionale di Geofisica e Vulcanologia of Catania (INGV-CT), with that collected by satellite-based sensors. The ground-based cameras provide both thermal and visible images and, for our study, were supplemented by use of thermal images collected during ground-based surveys carried out to map the lava flows. The satellite data are taken from MSG's SEVIRI sensor, a sensor that provides infrared data every 15 minutes and allows us to obtain the time-averaged discharge rates (TADRs) during short-lived lava fountain events [*Harris et al*., 2011; *Vicari et al.*, 2011]. In addition, $SO_2$ released by open vent degassing at the summit craters, and recorded by the FLAME scanning ultraviolet spectrometer network [*Salerno et al*., 2009a, 2009b] were available, along with FTIR measurements collected before and after the eruptive phase. These near-infrared-to-ultraviolet remote sensing measurements were used to estimate degassing rates and the volume of magma intruded within the system, as well as to track the gas flux and composition before, during, and after the 11-13 January 2011 lava fountain event. This integrated remote sensing data set allowed us to reconstruct the eruptive sequence, quantify the erupted

volume, and compare the erupted and intruded magma volumes, thus allowing us to constrain the eruptive processes taking place in the feeder conduit and to improve our ability to forecast and track future explosive events.

## 2. Recent eruptive events at Etna

The recent eruptive history of Etna volcano has been characterised by frequent effusive episodes, with more than 40 flank eruptions occurring during the 20$^{th}$ century [e.g. *Andronico and Lodato,* 2005; *Branca and Del Carlo*, 2005]. Explosive eruptions have also been common, and are of some concern due to the hazard posed by the associated ash plumes: the 2001 and 2002-2003 eruptions both caused severe disruption to Catania's international airport. During both events eruptive columns spread ash all over southern Italy [*Calvari et al*., 2001; *Behncke and Neri*, 2003; *Andronico et al*., 2005], with some ash reaching Cefalonia in Greece, 500 km away [*Dellino and Kyriakopoulos,* 2003]. The last effusive event occurred in 2008-2009, and comprised an initial phase of lava fountaining that fed an eruptive column, and was accompanied by lava flows that spread within the Valle del Bove (VdB), reaching over 6 km in length [*Bonaccorso et al*., 2011a, 2011b]. Following this eruption, the volcano remained largely quiescent until 2010, during which time its summit craters were actively degassing. A first explosive phase occurred at the SE-Crater (SEC; Fig. 1c) on 8 April 2010, and produced an ash plume that covered the uppermost NE sector of the volcano with ash, and a small pyroclastic flow. On 25 August 2010 another intense explosive phase occurred at the Bocca Nuova crater (Fig. 1c). This was characterised by an ash emission that lasted several seconds and spread ash over the uppermost flanks of the volcano. Weaker explosive phases were recorded during December 2010 from a depression (pit crater) on the E flank of SEC at 3050 m a.s.l. (Fig. 1c), and on 2 January 2011 a further explosive event was observed at this site. Explosions continued until 3 January, and were characterised by pulsating gas

bursts, red-glowing at night and sometimes accompanied by small ash emissions. This explosive activity stopped on 3 January and resumed on 11 January, when a short but intense eruptive phase began at SEC. The eruptive activity that occurred between 11 and 13 January is the topic of the present paper.

## 3. Methods

### 3.1 Thermal and visible camera network

Mount Etna's camera network consists of thermal and visible cameras that allow continuous, real-time ground-based imaging of the volcano activity every 1-2 sec [e.g. *Andò and Pecora*, 2006; *Behncke et al*., 2006, 2009]. The network consists of two thermal cameras, EMOT and ENT, and five visible cameras: EMOV, ENV, EMV, ESV, and ECV (see Fig. 1 and Tab. 1 for locations).

EMOT and ENT are equipped with an A320 and an A40M Thermovision Forward Looking InfraRed (FLIR Systems) camera, respectively. Both record in the 7.5 and 13 μm spectral range, providing 320 × 240 pixel images with a spatial resolution of 1.3 μrad. The A320 and A40M have thermal sensitivities of 70 mK at 30°C, and 80 mK at 25°C, respectively. While EMOT thermal images are displayed with a fixed colour scale that ranges between -20 and 60°C, ENT images are displayed with a fixed colour scale with a range of -10 and 60°C. Radiometric data, recorded between 0 and 500°C, are processed in real-time by custom written code (NewSaraterm) [*Behncke et al*., 2009]. The visible cameras at EMOV, ENV, ECV, and EMV consist of a Canon VC-C4 with a 16× optical zoom lens. This camera provides a horizontal field of view (FOV) of between ~3 and 47.5° (Tab. 1). The visible camera at ESV is a Sony FCBEX 480 CP with FOV of between ~2.8 and 48° (Tab. 1). Given the variable focus of the visible cameras (Tab. 1), to calculate the size of any object within the FOV we used reference distances between known targets within each image. For night-time images recorded by

ECV, we used the vertical distance between the pit crater and the Rifugio Sapienza tourist facility (1920 m a.s.l.; Fig. 1). This yielded a vertical distance of 1130 m and was used to estimate the ash column height as well as the length of the lava flows spreading towards the east until they reached ~2170 m a.s.l.. At this elevation the VdB rim hides the lava flows from the ECV camera view.

EMOT (Fig. 3), EMV (Fig. 4) and ECV (Fig. 5d-f) provided the best quality information and images during the 11-13 January eruptive event. In particular, using images from EMOT we derived the frequency of the strombolian activity by manually counting the number of explosions across 15 min time windows (the duration of each archived video clip). The frequency of strombolian bursts increased to a point at which the discrete bursts became uncountable. At this point we measured the height, width and area of the saturated portion of the explosive cloud. Images provided by EMV allowed us to derive the area covered by the upper portion of the lava flow field (up to ~2200 m a.s.l.) and to track its stagnation and cooling (Figs. 4a-h; 6b). They also allowed us to observe the ash emissions that followed the end of the fountaining event (Fig. 4i). Images from EMOT and ECV allowed tracking of the explosive activity (Fig. 6a), with ECV providing an almost complete view of the ash column emitted by the lava fountain. ENT also showed both the lava fountains and associated ash columns, as well as dust clouds rising above the active lava flow fronts (Fig. 5g-j).

### 3.2 Thermal surveys

Ground-based thermal surveys, carried out on 13 and 14 January 2011, allowed imaging of the lower part of the lava flow field, i.e., that spreading below 2200 m a.s.l. within VdB (Fig. 2). The camera used was a FLIR SC660 hand-held thermal camera. This camera consists of a 640 × 480 uncooled microbolometer-detector array sensitive across the 7.5-13 μm spectral range. It has a 18 × 24° FOV, records temperature with a precision of ±1% (±1°C) and has a sensitivity of 0.08°C at 30°C. The camera allows recording of images in three temperature ranges: -40 to 120°C, 0 to 500°C and 350 to

1500°C, at time steps of up to 30 Hz. Thermal imagery of the lava flow field was collected using the middle range (0-500°C) at a frame rate of 4 images per sec. Air temperature and relative humidity were recorded simultaneously with thermal imagery and used to apply a first-order correction for atmospheric effects. For emissivity we have used 0.98 [*Buongiorno et al*., 2002]. See *Spampinato et al*. [2011] for full review of thermal camera operation and data processing for volcanological applications.

### 3.3 Gas flux measurements

$SO_2$ flux at Mount Etna is measured by the FLAME (FLux Automatic MEasurement) network of scanning ultraviolet spectrometers [*Salerno et al*., 2009a]. The network consists of eight stations spaced ~7 km apart and installed at an altitude of ~900 m a.s.l. on Etna's southern, eastern and northern flanks (Fig. 1). During daylight, each device scans the sky in a vertical plane over 156° (almost horizon-to-horizon) intersecting the plume at a distance of ~14 km from the summit region. In each scan, 104 open-path ultraviolet spectra are collected. $SO_2$ slant column densities are reduced from each spectrum following the Differential Optical Absorption Spectroscopy (DOAS) methodology [e.g. *Plat and Stutz*, 2008] using a modelled reference spectrum [*Salerno et al*., 2009b]. $SO_2$ column densities are then transmitted by FreeWave radio-modem to INGV-CT, where $SO_2$ mass flux (in Megagram per day, Mg $d^{-1}$) is computed in real-time.

HCl and HF fluxes were calculated by combining the $SO_2$ flux with the molar ratios of $SO_2$/HCl and $SO_2$/HF measured during daily surveys. Ratios were determined from solar occultation open-path Fourier Transform InfraRed (FTIR) spectra, in which the infrared source was the sun and the gas plume was interposed between the sun and the spectrometer, following the methods of *Francis et al*. [1998]. Spectra were collected with a Bruker OPAG-22 spectrometer with a ZnSe beam splitter and a 0.5 $cm^{-1}$ resolution. The detector was a liquid nitrogen-cooled Mercury-Cadmium-Telluride (MCT) sensitive between 1000 and 6000 $cm^{-1}$. The gas column amounts were retrieved using a non-linear least square

fitting program based on the Rodgers optimal estimation algorithm [*Rodgers*, 2000] and the Oxford Reference Forward Model (RFM) radiative transfer model (http://www.atm.ox.ac.uk/RFM/), using line parameter data from the HITRAN96 molecular spectroscopic database [*Rothman et al*., 1998]. Solar occultation mode provides information on the concentrations of $SO_2$, HCl and HF, which are three gas species with negligible concentrations in the free troposphere, but which are abundant within volcanic plumes [e.g. *Sparks et al*., 1997]. The uncertainty on retrieved gas amounts was calculated using the residual of the least square fitting, and was ~4%. Ratios were determined by measuring 100 or more spectra. The retrieved amounts of $SO_2$ were then plotted against HCl and HF. The gradient of the resulting linear regression plots give the ratios of $SO_2$/HCl and $SO_2$/HF [e.g. *La Spina et al*., 2010].

### 3.4 Satellite data

The satellite time series comprised the full archive of MSG-SEVIRI data acquired during the lava fountaining phase by the direct reception capability at the Observatoire de Physique du Globe de Clermont-Ferrand (OPGC, Clermont Ferrand, France). The SEVIRI (Spinning Enhanced Visible and InfraRed Imager) sensor is flown on the Meteosat Second Generation (MSG) satellite. This flies in a geostationary orbit above the Equator over Africa at an altitude of 35,000 km. From its equatorial location, SEVIRI can image Etna once every 15 minutes. Thus we built a time series of 96 images for the 24 hour period spanning the main lava fountain phase. We use data collected in SEVIRI's IR3.9 (3.48-4.36 μm) and IR12 (11.00-13.00 μm) channels. While the wavelength of the IR3.9 channel is sensitive to sub-pixel hot spots, that of IR12 is useful for characterising the temperature of the ambient background [e.g. *Wright and Flynn*, 2004]. Both channels have a spatial resolution of 3 km. Radiance data from all hot spots identified in the IR3.9 channel, corrected for atmospheric, surface emissivity and reflection effects, were used to estimate the heat flux and lava discharge rate for the active, and cooling, flow field following a modified version of the methodology of *Harris et al*. [1997]. The full

methodology as applied to the SEVIRI data is described in *Gouhier et al*. [2011, submitted] and *Vicari et al.* [2011].

## 4. The 11-13 January eruptive episode

Figure 2 shows the main area impacted by the eruption, showing the SEC, the pit crater responsible for the eruptive events described here, the lava flow field emplaced within the VdB, and the summit area of Mount Etna (in the background). The eruptive activity began at the pit crater on 11 January, though poor weather conditions permitted its observation only from EMOT and then only after 17:50 (all times reported are UTC). The eruption fed strombolian activity that was initially confined to the pit crater (Fig. 2), as evident from observed glow (red in Fig. 3a). Between 20:30 and 21:45, the number of explosions increased and the frequency became quite regular (Fig. 6a), with explosions reaching a height of ~30 m above the pit rim at 23:30. After this peak, both the frequency and intensity of the events decreased to a lower, but steady level, before decreasing further between 00:45 and 01:30 on 12 January. The frequency of explosions increased again later in the morning (especially between 09:45 and 10:00; Figs. 3a, 6a) with spatter being erupted from two vents. Strombolian activity intensified further between 17:45 and 18:00 with ejecta being emitted in several directions and bombs falling well beyond the pit crater rim (Figs. 3b, 6a). By 18:38 we could not distinguish the vents; this suggested that the temperature within the pit crater was so high that the two vents had formed a unique saturated area as visible from EMOT (Fig. 3c). After ~19:15 the lower sector of the pit also began to produce occasional explosions, with activity at up to three explosive vents. At 20:20, lava began to flow from the lower rim of the pit crater (Fig. 4a), which slowly spread towards the SE. At 20:49 a second lava flow covered the upper part of the lava channel feeding the initial flow, and the explosion frequency and ejects height increased (Fig. 4b).

After 21:15 explosions became almost continuous (Figs. 3c-d), suggesting shift from strombolian to a transitional eruptive style [e.g. *Parfitt*, 2004; *Spampinato et al*., 2008]. At 21:27 explosive activity increased further (Fig. 4c), and a third lava flow appeared, while spatter were covering the upper part of the lava flow field. About 15 minutes later, the new lava flow was followed by a fourth flow. This new flow spread over the uppermost portion of the channel that fed the previous flows, and large incandescent blocks detached from the flow front to roll off down slope. Between 21:44 and 21:47, spatter began to cover most of the northern outer flank of the SEC. Coverage was sufficient so as to form a rheomorphic or rootless lava flow [*Head and Wilson*, 1989]. Meanwhile, the pit crater began to feed a fifth lava flow (Fig. 4d). At this point, the velocity and forward propagation of the lava flow fronts was observed to increase steadily (Fig. 6b), and the height of the ash column grew (Figs. 5a-b, Tab. 1).

At ~21:50, spattering from the pit crater became steady and the emission style evolved to fountaining (Figs. 3e, 5g, 5j). Two minutes later, both the height of the lava fountains and ash column increased significantly, with most of the tephra spreading SSW (Figs. 3e, 4e, 5c). Increased explosive activity was accompanied by collapses on the southern flank of the SEC. By 21:59 a thick ash plume was apparent (Figs. 3f, 4f, 5e), and the lava flow field within the VdB continued to spread in three branches (Fig. 4f). A second rootless flow also began to form due to tephra remobilization in the same site as the previous rheomorphic flow (Fig. 4f). Explosive activity peaked between 22:00 and 23:00 on 12 January when the maximum height of the lava fountains reached ~800 m above the pit (cfr Figs. 3 and 4), and the apparent temperature recorded by ENT increased from ~80°C to 120-160°C (Fig. 5j). By 22:05 four lava flows were spreading down the western flank of the upper VdB. At this time, the lava fountains also expanded eastward (Figs. 3e-f) and became higher. Increased explosive and effusive activity was accompanied by erosion of the eruptive vent. By 22:20 lava fountains widened further and also became taller (Figs. 3f-g, 6b). At 22:29 two main jets could be distinguished suggesting that two

explosive vents were still active within the pit crater (Fig. 4g). Successively, more flows covered the upper part of the lava flow field which, between 22:00 and 23:30, reached its largest active area (Fig. 6b). Three more lava flows erupted at ~22:42, 22:59, and 23:13, to feed a final total of nine lava flows (Figs. 3g-i).

After 23:10 the lava fountaining intensity decreased substantially (Figs. 3j-l, 4h, 5j, 6b), with the last small vertical jet of lava showing an apparent eastward displacement of the explosive vent by ~110 m to the E, due to widening of the pit rim. This modified vent location was also ~30 m lower than that of the initial vent (Figs. 3b-l). This outline pit crater enlargment was directly observed during an overflight in the following days. After 23:24 lava output also declined and the distal portion of the lava flow field began to cool (Figs. 4h, 5j, 6b). Lava flows were still active on the N flank of SEC, though, probably fed by collapse of hot tephra emplaced during the lava fountaining phase. Slow movements of the lava flow fronts continued until ~23:59.

At midnight, the eruptive activity returned to strombolian style, with a few discrete explosions feeding small lava flows that covered the proximal lava flow field to the E and S. At ~00:25 on 13 January shallow explosions at the pit crater were observed. These produced a hot gas cloud that rose several hundred meters. Collapses were apparent at the lava flow fronts of the shorter S and N flows emplaced on the flanks of the SEC. These were probably caused by destabilization of the eruptive products on the steep slopes of the SEC, as has often been observed at Etna after major explosive phases [e.g. *Calvari and Pinkerton*, 2002; *Behncke et al*., 2003].

After 00:55 the flow field within the VdB displayed considerable surface cooling (Fig. 6b), although the N and S flows on the SEC flanks were still slowly moving as the channels drained. At 01:00 glow from the pit crater also waned significantly. By 02:17, all lava flow movement had halted (Fig. 6b), even if localised flows and collapses of the flow fronts were observed until ~06:00;

representing post-emplacement reorganisation of the lava flow field. Explosive activity at the pit crater was over by 04:15.

Between 06:15 and 06:45 only impulsive degassing (gas puffing) was observed, and between 07:22 and 07:35 pulsating dark ash plumes were emitted from the pit. These were likely from collapses inside the crater, but were possibly associated to deep explosive activity. After 08:17 ash became reddish and more dilute, with emission continuing until 09:22 and suggesting collapses within the pit crater following drainage [e.g. *Bertagnini et al*., 1990; *Calvari and Pinkerton*, 2004]. No further emissions from the pit crater were detected after ~13:00 on 13 January.

## 5. Results

### 5.1 Gas flux between 2 and 19 January 2011

Figure 7 shows both long and short-term variations in the 7-day-running mean of the $SO_2$, HCl and HF fluxes, with the long-term plot spanning May 2010 to January 2011. Overall, the three gas species showed correlated behaviour, though sometimes they displayed decoupling. Note that, in Figure 7a, in order to plot both the HCl and HF fluxes together on the secondary y-axis, we have had to multiply the HF flux by 5. Hence, in Figure 7a the real values of HF are actually a fifth of the fluxes plotted. Between May 2010 and July 2010, $SO_2$, HCl and HF fluxes showed trends which remained steadily confined within 1300-2400 Mg $d^{-1}$, 130-260 Mg $d^{-1}$, and 118-136 Mg $d^{-1}$ for the three species, respectively (Fig. 7a). From the second half of July 2010, the three geochemical signals displayed pulsating but increasing trends, that concordantly climaxed in November 2010, when fluxes reached 4800, 963, and 640 Mg $d^{-1}$ for $SO_2$, HCl and HF, respectively (Fig. 7a). After this period the three emission rates declined to values of 1500, 314, and 123 Mg $d^{-1}$ by January 2011 (Fig. 7a).

Figure 7b is a zoom that details the gas flux temporal variations between 2 and 19 January 2011, a period including the eruptive phase. During these 18 days of observations, the $SO_2$ fluxes were constantly recorded, except on 1, 3 and 4 January when the wind (and thus plume) direction was towards a sector of the volcano not covered by the FLAME network. The daily averaged $SO_2$ emission rates varied between a minimum of 500 Mg $d^{-1}$ (on 19 January) and a maximum of 3400 Mg $d^{-1}$ (on 8 January), with the mean daily $SO_2$ emission rate being 2000 Mg $d^{-1}$ (standard deviation, $1\sigma$ = 800 Mg $d^{-1}$). Figure 7b shows three main peaks on 8, 11 and 13 January, when mean daily $SO_2$ emission rates of over ~3000 Mg $d^{-1}$ were recorded. These are followed by a generally decreasing trend, with $SO_2$ fluxes decreasing to ~500 Mg $d^{-1}$ by 19 January.

The HCl and HF fluxes were obtained by FTIR measurements on 11 and 14 January, respectively (i.e. before and after the 11-13 January 2011 eruptive episode). The $SO_2$/HCl and $SO_2$/HF molar ratios were 2.5 and 6.6 on 11 January, and 2.9 and 16.3 on 14 January, resulting in HCl and HF fluxes of 470 and 100 Mg $d^{-1}$ on 11 January, and 300 and 30 Mg $d^{-1}$ on 14 January. Both HCl and HF fluxes then show a marked decline between 11 and 14 January.

Figure 7c displays a further zoom, plotting the daily averaged $SO_2$ fluxes measured (during daytime) between 10 and 14 January, and thus recorded before and after the main eruptive event of 12 January. Over this period, the $SO_2$ flux shows a cyclic pattern, with maxima recorded on 11 and 13 January (when values peaked at 5000 and 4200 Mg $d^{-1}$, respectively) and a minimum of 650 Mg $d^{-1}$ on 12 January (Fig. 7c). On 10, 12, 13, and 14 January the variance was approximately half that measured on 11 January. Knowing the total elemental sulphur released between 1 August 2010 and 10 January 2011 by $SO_2$ flux measurements, the cumulative quantity of degassed magma was calculated following *Allard* [1997]. This yielded a volume of ~$32 \times 10^6$ $m^3$.

### 5.2 Strombolian and lava fountain activity

During the morning of 11 January, the pit crater on the E flank of the SEC started to show pulsating degassing, with explosive activity first observed at 17:50 the same day. Figure 6a displays the number of explosions with time. An overall generally increasing trend can be seen after 00:45 on 12 January, which is overprinted by cycles of waxing and waning activity lasting 3-4 hours and increasing in wavelength with time (Fig. 6a). No data were available between 10:30 and 16:00 due to obscuration by thick meteorological clouds. After 20:15 the strombolian activity passed to transitional, with explosions being so continuous that they were almost uncountable (Fig. 5j). After ~21:50 the transitional style changed to lava fountaining (Figs. 3d-e, 4d-e, 5b-c, 5j). Thus, from 21:15 onwards we measured the height, width and area occupied by the lava fountains as seen from the two positions of EMV and EMOT (Figs. 4c-h, 6b, 8a-c). We note that, although not measuring exactly the same parameter, the heights measured from the two locations show comparable values, although at times EMOT recorded lower values. We interpret this as being due to ash fallout obscuring the fountain from the EMOT thermal camera view. Fountain activity ceased at 23:50, having lasted 2 hours and 35 minutes. The maximum height reached by the lava fountains was between 750 m (measured from EMV) and 830 m (measured from EMOT) and occurred at 22:21 on 12 January (see also Fig. 6b). Maximum fountain width was recorded at between 420 m (measured from EMV) and 516 m (measured from EMOT), with peaks of up to 550 m (Fig. 8b). During the peaks the presence of fallout was adding to the apparent width of the eruptive column, making the EMOT measurement larger than the EMV measurement (which was not so affected by fall out). Between 21:56 and 22:59, the estimated height of the ash column rising above the fountain, measured from ECV, was ~6 km (Figs. 5d-f). This value has to be considered a minimum because this height marks the upper limit of our FOV, and the ash continued to rise upwards and out of the camera FOV. The ash column then drifted SSW in the wind. By 23:00 the lava fountaining was declining, with heights to ~200 m. We selected 53 frames from EMV and the corresponding 53 frames recorded from EMOT at time intervals of 180 seconds. We then extracted the

lava fountain heights from the mean value of each pair of frames. We use these values to estimate initial velocity at the vent ($v_0$) to account for the measured height (h), using:

$$v_0 = \sqrt{(2gh)} \quad (1)$$

Derived velocities span 33 m $s^{-1}$ at 21:15 to 125 m $s^{-1}$ at 22:21. After this time there was a gradual decrease in the velocity until midnight, corresponding to the decline in the maximum height of the lava fountains. Using ground- and helicopter-based photos collected by INGV-CT during surveys following the eruptive episode, we estimated a diameter for the vent at the bottom of the pit crater of ~30 m. We used this value to estimate vent area assuming a circular shape which, with the exit velocity of the ejecta, allows us to calculate the volume flux of magma passing through the vent to feed the lava fountains. The total erupted volume of vesiculated material is then obtained from integrating these volume fluxes through time. Given that this was vesiculated material, and that the lava fountain jets comprised a mixture of pyroclasts and gases, to obtain the dense rock equivalent (DRE) erupted volume we assumed that the jet comprised 0.35% of magma. This value is suggested by *Parfitt* [2004] as being typical for lava fountains, such as those occurred at Kīlauea in 1983 [*Wolfe et al*., 1988]. The resulting DRE volume erupted during the 2 hours and 35 minutes of lava fountaining is ~$0.85 \times 10^6$ $m^3$, giving a mean output rate of ~92 $m^3$ $s^{-1}$ for just the pyroclastic portion of this eruptive event. This result is in good agreement with estimates obtained during previous lava fountaining events at Etna [e.g. *Behncke et al*., 2006] and has to be considered a minimum value for the entire episode, because it does not take into account the tephra erupted during the 26 hours of strombolian activity that preceded the lava fountaining phase.

### 5.3 Lava flow field

The emplacement of the upper lava flow field across the western headwall of the VdB was tracked and quantified using images recorded by EMV (Figs. 4a-i, 6b). In carrying out this analysis, we have to bear in mind that the portion of the lava flow field that spread beyond the EMV FOV was not included in the image (Fig. 4). Thus, the flow field area below the ~2200 m elevation was not accounted for in this analysis. Using NI Vision Assistant software we selected a fixed colour threshold to crop the whole lava flow field in each image. We then used this to calculate the area covered by active lava flows, and thus to quantify the change in area covered by active lava flows with time (Fig. 6b). The length of the active lava flows was obtained from ECV, which provided a side view until ~22:00, when the flows began spreading within the VdB. Thus, although the complete development of the lava flow field could not be observed, we do have a rather good description of the growth of the uppermost three-quarters of it (Fig. 6b). The area covered by the active lava flows displays two peaks at 22:25 and 22:40. Considering that lava fountain area peaked at 22:15 and 22:24 (Figs. 6b, 8c), it is thus possible that each peak in the lava fountain area is related to a subsequent peak in the lava flow field area. In fact, we observed that rapid accumulation of spatter on the upper part of the SEC cone, and on the upper portion of the lava flow field, was followed by remobilization of this loose material to form rootless flows which increased the supply to the flow field.

The first lava flow emerged from the lowest point on the pit crater rim at 20:20 on 12 January, and lava flow fronts stopped final movement at 02:17 on 13 January, giving a total emplacement time of ~6 hours. Ground-based thermal imagery collected during the mornings of 13 and 14 January 2011 from the S rim of the VdB showed that the stationary flow fronts were located at ~1650 m a.s.l. (Figs. 2, 9). At the time of the thermal surveys, the lava flow field displayed low temperatures, with maximum temperatures across the distal area being between 330° and 430°C on 13 January and ~160°C on 14 January. The higher temperatures recorded on 13 January were due to lava channel drainage that locally disrupted the lava crust. At that time the lava front also experienced lateral

spreading, promoted by the low topographic gradient of the lower section of the VdB, as the flow field underwent post-emplacement reorganisation before finally solidifying. Oblique thermal imagery of the proximal area recorded on 14 January showed maximum apparent temperatures of ~200°C. During both surveys, no explosive activity from the SEC pit crater was observed, and maximum temperatures recorded on the eastern flank of the SEC on 14 January did not exceed 170°C.

The lava flow field displayed simple morphological structures, and lacked ephemeral vents, lava tubes or tumuli, in agreement with the morphology expected for short duration, high effusion rate flow [e.g. *Calvari and Pinkerton*, 1998, 1999; *Duncan et al*., 2004]. During the initial stages of lava output, the lava flow spread at low rate, and displayed surface structures similar to large-scale folds. The supply to the lava flow field then increased due to the contribution of the fallout from the lava fountain (Fig. 6b), as well as by overflow from the pit crater that eventually formed nine lava flow units that overlapped along the upper part of the S lava channel. These flow units overlapped with the rheomorphic or rootless flows resulting by flowage of the proximal spatter covering the flanks of SEC (Fig. 12).

Maximum (final) lava flow field area and length were derived using thermal and visible images obtained from a helicopter survey on 19 January, and were 1.07 $km^2$ and 4.3 km, respectively [*Behncke et al*., 2011; Figs. 2, 9]. Using this area, with a minimum and maximum bound on the mean flow field thickness of 1 and 2 m, and an average vesicularity of ~22% [*Harris et al*., 2005], we obtained a DRE volume of the lava flow field between ~0.83 and 1.77 × $10^6$ $m^3$, resulting in mean output rates for the lava flow field of between ~38 and 77 $m^3$ $s^{-1}$. Considering also the DRE volume of pyroclastics erupted (~0.85 × $10^6$ $m^3$), we obtain a total erupted DRE volume (for all products: lava + pyroclasts) of between ~1.7 and 2.5 × $10^6$ $m^3$, of which the pyroclastic component comprised ~20%. The total volume yields a mean output rate for pyroclastics and lava at between 78 and 116 $m^3$ $s^{-1}$.

### 5.4 SEVIRI-derived heat flux trend and TADR measurements

The onset of effusive activity was apparent in the SEVIRI data from a hot spot that developed from 20:00 onwards on 12 January. The heat flux continued to wax through 21:00 when the hot spot became obscured by the plume associated with the most explosive phase of the episode (Fig. 10). By the time the plume cleared to allow the hot spot to be detected once more, lava flow activity had reached such an extent that the IR3.9 data were saturated. Termination of saturation at 01:00 coincides with the termination of supply to the lava flow field from the vent. Thereafter we recorded a cooling curve, as the flows stagnated and began to cool, with the hot spot becoming unresolvable by 11:00 on 13 January (Fig. 10). This trend has also been reported by *Vicari et al.* [2011]. Perturbations in the otherwise smooth cooling curve, such as those apparent during 03:00 and 04:00, may be due to late stage flows as the lower sections of the channels drained and the flow field underwent a final re-organisation.

Converting the heat flux to a TADR for the eruptive period of the time-series, i.e. between 20:00 and 01:00, yields a TADR that climbs to ~15 $m^3$ $s^{-1}$ during the first hour and a half of effusion (Fig. 10). Thereafter, the record has a gap, during which time the flow field was obscured by the overlying plume until ~23:00. At this point we record a minimum possible value (capped by saturation) of ~30 $m^3$ $s^{-1}$. Obscuration by the plume, as well as saturation, during the period of peak discharge mean that time-integration of TADRs to obtain total effused volume will yield an underestimate [*Gouhier et al*., 2011, submitted]. Therefore, we modified the approach of *Wooster et al.* [1997] to estimate the total effused volume. *Wooster et al.* [1997] integrated heat fluxes obtained from satellite thermal data during the cooling phase of Etna's 1991-1993 flow field to obtain the total power generated by the lava during cooling. Given a cooling curve, we can thus integrate the heat flux through time to estimate the total power released (in Joules) by the cooling lava. This can, in turn, be converted to the mass or volume of lava that needs to be cooled in order to liberate that power [see

*Rowland et al.*, 2003]. This conversion methodology, as applied to the SEVIRI data, is explained in *Gouhier et al.* [2011, submitted].

By integrating the power under the cooling curve we obtain a value for the total power release during cooling of 460 GJ. Converting this to a volume of lava that needs to be cooled by 50°C, we obtain a lava volume of $1.2 \times 10^6$ m$^3$ [*Gouhier et al*., 2011, submitted]. Distributing this volume over the period of effusion, and removing the volumes known to be erupted during the ash-cloud-free phase, we find that 83% (or $10^6$ m$^3$) of the total volume was erupted during the period of peak effusion that spanned 21:30 - 01:00. This gives a TADR over this 3.5-hour-long period of peak effusion of 80 m$^3$ s$^{-1}$. By comparison, ground-based thermal camera measurements yielded a total DRE volume of 1.7-2.5 $\times$ $10^6$ m$^3$, which is roughly in agreement with that calculated using the satellite data, as well as that calculated by *Vicari et al.* [2011] using the same SEVIRI data set. As discussed by *Gouhier et al.* [2011, submitted], the discrepancy may be explained by some uncertainties on parameters used at the input of the satellite-based retrieval scheme, or error in the thickness assumption used for the thermal-camera-based extraction. However, these results show that comparable volumes are obtained using three independent methods. This lends confidence to the measurement.

## 6. Discussion

Etna's 11-13 January 2011 eruptive phase was observed by a plethora of remote sensing techniques that allowed us to track and quantify the trends in the explosive and effusive activity before, during and after a lava fountain event. The mean output rates of 78-116 m$^3$ s$^{-1}$ for the 6-hour-long fountain event are quite high when compared with those experienced during longer-duration flank and summit effusive eruptions at Etna [e.g. *Calvari et al*., 1994; *Harris et al*., 2000; *Calvari et al*., 2003; *Harris et al*., 2011]. However, they are consistent with rates estimated during other short-lived lava fountaining

events at Etna, especially those that preceded the 2001 flank eruption [*Harris and Neri*, 2002; *Behncke et al*., 2006]. In 2000, Etna witnessed 64 lava fountains each lasting no more than 30 minutes [*Alparone et al*., 2003; *Behncke et al*., 2006]. These culminated in the 2001 flank eruption [*Calvari et al*., 2001; *Behncke and Neri*, 2003]. A similar activity pattern also preceded the 2002-2003, 2006, and 2008-2009 effusive eruptions [*Andronico et al*., 2005; *Neri et al*., 2006; *Spampinato et al*., 2008; *Bonaccorso et al*., 2011a, 2011b]. The occurrence of an intermittent phase of explosive activity prior to the aforementioned eruptive events, suggests that the January 2011 episode might represent the start of a new eruptive cycle. In fact, the sequence of eruptive events here described is typical of many other eruptions at Etna [e.g. *Alparone et al*., 2003; *Allard et al*., 2005; *Behncke et al*., 2006], when the intrusion of a gas-rich batch of magma into the shallow feeder system initiates a new cycle. Intrusion is followed by the renewal of explosive activity at one or more of the summit craters [e.g. *Andronico et al*., 2005; *Burton et al*., 2005].

Intermittent explosive events at Etna are usually preceded and/or accompanied by major changes in the volcanic gas composition and flux rates [e.g. *Caltabiano et al*., 1994, 2004; *Andronico et al*., 2005; *Burton et al*., 2005; *Salerno et al*., 2009a]. Magma contains dissolved volatiles ($H_2O$, $CO_2$, S, Cl, F, etc.) with different solubilities, each of which gradually reaches a saturation pressure and exsolves into a separate magmatic gas phase (bubbles) during magma ascent [e.g. *Anderson*, 1975; *Carroll and Holloway*, 1994; *Oppenheimer*, 2003]. Thus, during magma ascent towards the surface, the chemical composition of the gas phase changes following the pressure-controlled solubility of each volatile species, but also as a function of the dynamics of magma supply and ascent [*Burnham*, 1976; *Sparks*, 2003]. Melt inclusion studies indicate that S, Cl and F start to exsolve at confining pressures of ~140, 100, and <10 MPa, respectively. These pressure values are equivalent to depths of ~4-5, 3, and 1 km, respectively [e.g. *Carrol and Webstar*, 1994; *Spilliaert et al*., 2006]. At Etna, prior to the 11-13 January 2011 lava fountaining event, significant temporal changes were observed in $SO_2$, HCl and HF

fluxes beginning in August 2010 (Fig. 7a), with the daily mean $SO_2$, HCl and HF fluxes displaying an increasing trend that peaked in November 2010. The progressive increase in gas fluxes likely marked the gradual supply of gas-rich magma into the shallow feeding system (1–4 km depth). After the November peak, gas fluxes gradually decreased reflecting a decline in the magma supply rate and the end of intrusion of volatile-rich magma into the shallow feeding system [*Allard et al.*, 2006; *La Spina et al.*, 2010]. Over the following two months, gas exsolution and bubble nucleation in the stored batch of magma would have led to volatile saturation and overpressure, the January 2011 eruptive activity being the result.

The January 2011 eruptive episode lasted ~32 hours, with the first 26 hours being characterised by increasing strombolian activity, passing into a six-hour-long transitional phase, to culminate with lava fountaining. Such behaviour is quite common at Etna, and normally marks the gradual transition from a two-phase slug flow regime to annular flow [e.g. *Jaupart and Vergniolle*, 1989; *Vergniolle and Mangan*, 2000; *Parfitt*, 2004]. Combining acoustic and experimental data, *Vergniolle and Ripepe* [2008] proved that, at Etna's SEC, a lava fountain results from a closely-spaced sequence of strombolian explosions that reflect the dynamics of a foam trapped in the crater reservoir, which is located at a depth of ~2 km [*Allard et al*., 2005; *Spilliaert et al*., 2006; *La Spina*, 2010], with more active foam coalescence occurring during lava fountaining when compared to strombolian activity.

The 11 January 2011 strombolian phase was characterised by linear growth in the number of events (by ~20 explosions every 4 hours). The constant rate of growth in the explosive activity with time implies a steady increase in gas exsolution from the conduit magma. Following the onset of strombolian activity, the $SO_2$ flux showed a pulsing decline until 11:00 on 12 January. This behaviour was independent from the explosive activity observed at the surface, which passed to transitional at 21:15 of 11 January. The period of low $SO_2$ flux marked a phase of poor degassing efficiency of the feeding system, as previously observed during Etna's 2002-2003 south flank eruption [*Spampinato et*

*al*., 2008]. On that occasion, the November 2002 lava fountaining phase was preceded by a decrease of the $SO_2$ flux, that then increased to record the highest peak ever measured at Etna only after the onset of lava fountaining [e.g. *Andronico et al.*, 2005; *Spampinato et al*., 2008; *Steffke et al.*, 2011]. Similarly, in 2011 the eruptive activity climaxed with lava fountaining, which was followed by high $SO_2$ flux values recorded the next day (on 13 January). The lava fountaining phase, in fact, may have renewed the degassing efficiency of the system. Once the degassing regime came back to its equilibrium, the $SO_2$ flux, as well as the HCl and HF fluxes, gradually declined to the pre-eruptive rates levels. This model suggests that the January 2011 eruptive event was fed by a small batch of gas-rich magma that had been stored in the shallow feeding system for at least two months prior to the eruptive event.

The 11-13 January fountain was also accompanied by lava output. This suggests that degassing of the stored magma also resulted in a volatile-depleted magma that accumulated in the shallow conduit. This magma was pushed out of the conduit, filled the pit crater and, eventually, overflowed from its lower rim. In fact, expansion of the lava volume stored in the shallow system, might have forced the degassed lava at higher levels in the conduit out of the vent and into the pit, in a process similar to that envisaged for gas-piston-related lava flow emplacement [*Johnson et al*., 2005]. Unloading of the magma column may have been aided by further decompression of the shallow feeding system. This likely led to development of trains of more closely-spaced slug sequences, that would have induced the change from strombolian, to transitional and, then, to lava fountaining activity. Similar to other short-lived eruptive events at Etna, the final stage of the activity was then characterised by crater wall collapses to produce reddish ash emissions, revealing conduit drainage, removal of crater-wall support, and collapse.

Based on previous eruptive cycles at Etna, the high intensity and the brief duration of the 11-13 January 2011 event leads us to propose that it was only the first episode of a sequence of paroxysmal

events that will, if the pattern of previous cycles repeats itself, culminate in a longer effusive eruption. Our assessments are supported by an estimate of the volume of degassed magma available for eruption, and that actually erupted so far. The amount of magma degassed between 1 August 2010 and 10 January 2011, and thereby assumed resident in the shallow system and available for eruption, is ~32 × $10^6$ $m^3$. If we compare this with the total volume (lava + tephra) erupted during the 11-13 January 2011 event (1.5-2.7 × $10^6$ $m^3$), we obtain a ratio between the intruded and erupted magma of between 10:0.5 and 10:1.0. Thus, only 5-10% of the available magma was erupted by the 11-13 January 2011 event, and ~32 × $10^6$ $m^3$ remains stored in the volcano's shallow supply system. At Etna, *Allard* [1997] and *Allard et al*. [2006] showed that, over long time-scales, only a small part of the total degassed magma is erupted, with the long-term ratio between degassed to erupted magma of ~4. Hence, considering the difference between the intruded and erupted magma volumes estimated here we propose that, in order to obtain the intruded/extruded ratio that characterises Etna, further paroxysmal eruptive events and/or a longer eruptive phase are required.

## 7. Conclusive remarks

The extremely short duration of Etna's 11-13 January eruptive episode meant that remote sensing data collected at high temporal resolutions from ground-based cameras and geostationary satellites were ideal for tracking its explosive and effusive character. Using a range of remote sensing data sets, we calculated that a total volume of ~1.7-2.5 × $10^6$ $m^3$ DRE was erupted in ~6 hours of intense explosive and effusive activity, with a TADR in the range ~78-116 $m^3$ $s^{-1}$. The building, pulsing pattern of strombolian activity observed in the preceding hours, suggested release of a small gas-rich batch of magma from a body previously intruded into the shallow system. The similarity between this event and others previously tracked on Etna, leads us to suggest that the January 2011 event may be the prelude

to a new phase of activity that may terminate in a longer, higher volume eruption. This hypothesis was partially supported by three additional eruptive events, all characterised by an initial explosive phase and followed by a short-lived fountaining and lava flow, that occurred on 18 February, 9-10 April, and 8-12 May 2011; while this manuscript was in review. These eruptive episodes were all fed by the same vent, i.e. the pit crater on the east flank of SEC. The January 2011 event was the strongest of these four events. If we make a rough estimate of the total erupted volume between January and May as being four times that erupted in January, we are still well below the ~4 ratio proposed by *Allard* [1997] and *Allard et al*. [2006], and thus can still expect for further eruptive events to follow shortly (three occurred on 9, 18-19, and 24-25 July 2011 while this manuscript was undergoing final checking by the co-authors).

**Acknowledgements**

The authors wish to thank Alfio Amantia for kindly providing his excellent airborne photos, Stefano Branca for the photo of Figure 9a, and Michele Prestifilippo for his assistance with the handling of camera videos and images. This paper benefited of discussions and data comparison with Alessandro Bonaccorso, Ciro Del Negro, Tania Ganci, and Anna Vicari. We acknowledge the precious work of the INGV-CT technical staff on the installation and maintenance of the camera network used here: Michele Prestifilippo and Francesco Ciancitto, and of those dealing with the FLAME network and FTIR measurements: Filippo Muré, Tommaso Caltabiano, and Daniele Randazzo. This manuscript benefited greatly from the encouragement, comments and suggestions of Alessandro Bonaccorso, Thor Thordarson, an anonymous reviewer, and the Editor André Revil.

**References**


Allard, P. (1997), Endogenous magma degassing and storage at Mount Etna, *Geophys. Res. Lett.*, *24*, 2219-2222.

Allard, P., M. Burton, and F. Muré (2005), Spectroscopic evidence for a lava fountain driven by previously accumulated magmatic gas, *Nature*, *433*, 407-410.

Allard P., B. Behncke, S. D'Amico, M. Neri, and S. Gambino (2006), Mount Etna 1993-2005: Anatomy of an evolving eruptive cycle, *Earth Sci. Rev*., *78*, 85-114.

Alparone, S., D. Andronico, L. Lodato, and T. Sgroi (2003), Relationship between tremor and volcanic activity during the Southeast Crater eruption on Mount Etna in early 2000, *J. Geophys. Res., 108* (B5), 2241.

Anderson, A.T. (1975), Some Basaltic and andesitic gases, *Rev. Geophys Space Phys*., *13*, 37-55.

Andò, B., and E. Pecora (2006), An advanced video-based system for monitoring active volcanoes, *Comput. Geosci*., *32*, 85– 91, doi:10.1016/j.cageo.2005.05.004.

Andronico, D., and L. Lodato (2005), Effusive activity at Mount Etna Volcano (Italy) during the 20th century: a contribution to volcanic hazard assessment, *Nat. Hazards*, *36*, 407-443, doi: 10.1007/s11069-005-1938-2.

Andronico, D., S. Branca, S. Calvari, M.R. Burton, T. Caltabiano, R.A. Corsaro, P. Del Carlo, G. Garfì, L. Lodato, L. Miraglia, F. Muré, M. Neri, E. Pecora, M. Pompilio, G. Salerno, and L. Spampinato (2005), A multi-disciplinary study of the 2002-03 Etna eruption: insights for into a complex plumbing system, *Bull. Volcanol*., *67*, 314-330, doi:10.1007/s00445-004-0372-8.

Andronico, D., and R.A. Corsaro (2011), Lava fountains during the episodic eruption South-East Crater (Mt. Etna), 2000: insights into magma-gas dynamics within the shallow volcano plumbing system, Bull. Volcanol., in print, doi. 10.1007/s00445-011-0467-y.

Behncke, B., M. Neri, and R. Carniel (2003), An exceptional case of endogenous lava dome growth spawning pyroclastic avalanches: the 1999 Bocca Nuova eruption of Mt. Etna (Italy), *J. Volcanol. Geotherm. Res.*, *124*, 115-128.

Behncke, B., M. Neri, E. Pecora, and V. Zanon (2006), The exceptional activity and growth of the Southeast Crater, Mount Etna (Italy), between 1996 and 2001, *Bull. Volcanol*., 69, 149-173, doi: 10.1007/s00445-006-0061-x.

Behncke, B., S. Branca, E. De Beni, C. Proietti, L. Spampinato, and M. Coltelli (2011), Cronologia dell'evento eruttivo del Cratere di Sud-Est avvenuto il 12/13 gennaio 2011 e mappatura del campo lavico, *INGV-CT, Internal Report*, Prot. int. n° UFVG2011/06, 4 pp.

Behncke, B., S. Falsaperla, and E. Pecora (2009), Complex magma dynamics at Mount Etna revealed by seismic, thermal, and volcanological data, *J. Geophys. Res*., *114*, B03211, doi:10.1029/2008JB005882.

Behncke, B., and M. Neri (2003), The July–August 2001 eruption of Mt. Etna (Sicily), *Bull. Volcanol., 65*, 461–476, doi:10.1007/s00445-003-0274-1.

Behncke, B., M. Neri, E. Pecora, and V. Zanon (2006), The exceptional activity and growth of the Southeast Crater, Mount Etna (Italy), between 1996 and 2001, *Bull. Volcanol*., *69*: 149–173, doi:10.1007/s00445-006-0061-x.

Bertagnini, A., S. Calvari, M. Coltelli, P. Landi, M. Pompilio, and V. Scribano (1990), The 1989 eruptive sequence, in *Mt. Etna: the 1989 eruption*, edited by F. Barberi, A. Bertagnini and P. Landi, pp. 10-22, CNR-GNV Special Issue, Giardini, Pisa.

Bonaccorso, A., A. Bonforte, S. Calvari, C. Del Negro, G. Di Grazia, G. Ganci, M. Neri, A. Vicari, and E. Boschi (2011a), The initial phases of the 2008-2009 Mt. Etna eruption: a multi-disciplinary approach for hazard assessment, *J. Geophys. Res.*, *116*, B03203, doi:10.1029/2010JB007906.

Bonaccorso, A., A. Cannata, R.A. Corsaro, G. Di Grazia, S. Gambino, F. Greco, L. Miraglia, and A. Pistorio (2011b), Multi-disciplinary investigation on a lava fountain preceding a flank eruption: the 10 May 2008 Etna case, *Geochem., Geophys., Geosyst*., doi:10.1029/2010GC003480, in print.

Branca, S., and P. Del Carlo (2005), Types of eruptions of Etna volcano AD 1670-2003: implications for short-term eruptive behaviour, *Bull. Volcanol*., *67*, 732-742.

Buongiorno, M.F., V.J. Realmuto, and D. Fawzi (2002), Recovery of spectral emissivity from thermal infrared multispectral scanner imagery acquired over a mountainous terrain: a case study from Mount Etna Sicily, *Remote Sens. Environ*., *79*, 123-133.

Burton, M.R., M. Neri, D. Andronico, S. Branca, T. Caltabiano, S. Calvari, R.A. Corsaro, P. Del Carlo, G. Lanzafame, L. Lodato, L. Miraglia, G. Salerno, and L. Spampinato (2005), Etna 2004-2005: An archetype for geodynamically-controlled effusive eruptions, *Geophys. Res. Lett., 32*, L09303, doi:10.1029/2005GL022527.

Caltabiano, T., R. Romano, and G. Budetta (1994), $SO_2$ flux measurements at Mount Etna (Sicily), *J. Geophys. Res., 99*, 12,809-12,819.

Caltabiano, T., M. Burton, S. Giammanco, P. Allard, N. Bruno, F. Murè, and R. Romano (2004), Volcanic gas emission from the summit craters and flanks of Mt. Etna, 1987-2000, in *Mt. Etna Volcano Laboratory, Geophys. Monogr. Ser*., vol. 143, edited by S. Calvari, A. Bonaccorso, M. Coltelli, C. Del Negro, and S. Falsaperla, pp. 111-128, AGU, Washington, D. C.

Calvari, S., and the whole scientific staff of INGV – Sezione di Catania (2001), Multidisciplinary Approach Yields Insight into Mt. Etna 2001 Eruption, *EOS Trans*., AGU, *82*, n. 52, 653-656.

Calvari, S., M. Coltelli, M. Neri, M. Pompilio, and V. Scribano (1994), The 1991-93 Etna eruption: chronology and lava flow field evolution, *Acta Vulcanol., 4*, 1-14.

Calvari, S., M. Neri, and H. Pinkerton (2003), Effusion rate estimations during the 1999 summit eruption on Mt. Etna, and growth of two distinct lava flow fields, *J. Volcanol. Geotherm. Res.*, *119*, 107-123, doi:10.1016/S0377-0273(02)00308-6, ISSN0377-0273.

Calvari, S., and H. Pinkerton (1998), Formation of lava tubes and extensive flow field during the 1991-93 eruption of Mount Etna, *J. Geophys. Res., 103* (B11), 27291-27302.

Calvari, S., and H. Pinkerton (1999), Lava tube morphology on Etna and evidence for lava flow emplacement mechanisms, *J. Volcanol. Geotherm. Res.*, *90*, 263-280.

Calvari, S., and H. Pinkerton (2002), Instabilities in the summit region of Mount Etna during the 1999 eruption, *Bull. Volcanol., 63*, 526-535.

Calvari, S., and H. Pinkerton (2004), Birth, growth and morphologic evolution of the "Laghetto" cinder cone during the 2001 Etna eruption, *J. Volcanol. Geotherm. Res.*, *132*, 225-239, doi:10.1016/S0377-0273(03)00347-0.

Carroll, M.R., and J.R. Holloway (1994), Volatiles in magmas, *Mineral. Soc. Am. Rev. in Mineral.*, *30*, 517.

Carroll, M.R., and J.D. Webster (1994), Solubility of sulphur, noble gases, nitrogen, chlorine, and fluorine in magmas, in *Volatiles in Magmas*, edited by M.R. Carroll, and J.R. Holloway, vol. 30, pp. 231-279, Mineral. Soc. Amer., Washington, D.C.

Dellino, P., and K. Kyriakopoulos (2003), Phreatomagmatic ash from the ongoing eruption of Etna reaching the Greek island of Cefalonia, *J. Volcanol. Geotherm. Res., 126*, 341-345.

Duncan, A.M., J.E. Guest, E. Stofan, S. Anderson, H. Pinkerton, and S. Calvari (2004), Development of tumuli in the medial portion of the 1983 aa flow-field, Mount Etna, Sicily, *J. Volcanol. Geotherm. Res.*, *132*, 173-187, doi:10.1016/S0377-0273(03)00344-5.

Ferrazzini, V., K. Aki, and B. A. Chouet (1991), Characteristics of seismic waves composing Hawaiian volcanic tremor and gas-piston events observed by a near-source array, *J. Geophys. Res.*, *96*, 6199- 6209.

Francis, P., M.R. Burton, and C. Oppenheimer (1998), Remote measurement of volcanic gas compositions by solar occultation spectroscopy, *Nature, 396*, 567-570.

Gouhier, M., A.J.L. Harris, P. Labazuy, Y. Guéhenneux, F. Donnadieu, S. Valade, and S. Calvari, (2011), Lava discharge during Etna's 11-13 January 2011 fire fountain event tracked using MSG-SEVIRI, *Geophys. Res. Lett*., submitted March 2011.

Harris, A.J. L., J. Bailey, S. Calvari, and J. Dehn (2005), Heat loss measured at a lava channel and its implications for down-channel cooling and rheology, *Geol. Soc. Am. Spec. Pap*er., *396*, 125-146.

Harris, A.J.L., A.L. Butterworth, R.W. Carlton, I. Downey, P. Miller, P. Navarro, and D.A. Rothery (1997), Low-cost volcano surveillance from space: case studies from Etna, Krafla, Cerro Negro, Fogo, Lascar and Erebus, *Bull. Volcanol., 59*, 49-64.

Harris, A.J.L., J.B. Murray, S.E. Aries, M.A. Davies, L.P. Flynn, M.J. Wooster, R. Wright, and D.A. Rothery (2000), Effusion rate trends at Etna and Krafla and their implications for eruptive mechanisms, *J. Volcanol. Geotherm. Res*., *102*, 237-270.

Harris, A.J.L., and M. Neri (2002), Volumetric observations during paroxysmal eruptions at Mount Etna: pressurized drainage of a shallow chamber or pulsed supply? *J. Volcanol. Geotherm. Res*., *116*, 79-95.

Harris, A., and M. Ripepe (2007), Temperature and dynamics of degassing at Stromboli, *J. Geophys. Res.*, 112, B03205, doi:10.1029/2006JB004393.

Harris, A.J.L., A. Steffke, S. Calvari, and L. Spampinato (2011), Thirty years of satellite-derived lava discharge rates at Etna: Implications for steady volumetric output, *J. Geophys. Res*., in print.

Head, J.W. III, and L. Wilson (1989), Basaltic pyroclastic eruptions: influence of gas-release patterns and volume fluxes on fountain structure, and the formation of cinder cones, spatter cones, rootless flows, lava ponds and lava flows, *J. Volcanol. Geotherm. Res.*, *37*, 261-271.

Heliker, C., and T.N. Mattox (2003), The first two decades of the Pu`u `Ō`ō - Kūpaianaha eruption: Chronology and selected bibliography. In: The Pu`u `Ō`ō - Kūpaianaha eruption of Kīlauea volcano, Hawai`i: the first 20 years. U.S. Department of the Interior, U.S. Geological Survey, USGS science for a changing world, Prof. Pap., 1676, 29-52.

Jaupart, C., S. Vergniolle (1988), Laboratory models of Hawaiian and Strombolian eruptions. *Nature*, *331*, 58-60.

Jaupart, C., and S. Vergniolle (1989), The generation and collapse of a foam layer at the roof of a basaltic magma chamber, *J. Fluid Mech*., *203*, 347-380, doi:10.1017/S0022112089001497.

Johnson, J.B., A.J.L. Harris, and R. Hoblitt (2005), Thermal Observations of Gas pistoning at Kilauea Volcano, *J. Geophys. Res.*, 110, B11201, doi:10.1029/2005JB003944.

La Spina, A. (2010), The magmatic plumbing system of Mt. Etna: insight by OP-FTIR observation, *PhD thesis*, University of Palermo.

La Spina, A., M.R. Burton, and G.G. Salerno (2010), Unravelling the processes controlling gas emissions from the central and northeast craters of Mt. Etna, *J. Volcanol. Geotherm. Res., 198*, 368-376.

Neri, M., B. Behncke, M. Burton, G. Galli, S. Giammanco, E. Pecora, E. Privitera, and D. Reitano (2006), Continuous soil radon monitoring during the July 2006 Etna eruption, *Geophys. Res. Lett., 33*, L24316, doi:10.1029/2006GL028394.

Neri, M., F. Mazzarini, S. Tarquini, M. Bisson, I. Isola, B. Behncke, and M.T. Pareschi (2008), The changing face of Mount Etna's summit area documented with Lidar technology, *Geophys. Res. Lett., 35*, L09305, doi:10.1029/2008GL033740.

Oppenheimer, C. (2003), Volcanic degassing, in *The Crust, Treatise on Geochemistry*, vol. 3, edited by R.L. Rudnick, H.D. Holland, and K.K. Turekian, pp. 123-166, Elsevier-Pergamon, Oxford.

Parfitt, E.A., and L. Wilson (1995), Explosive volcanic eruptions: IX. The transition between Hawaiian-style lava fountaining and Strombolian explosive activity. *Geophys. J. Int.*, *121*, 226-232.

Parfitt, E.A. (2004), A discussion of the mechanisms of explosive basaltic eruptions, *J. Volcanol. Geotherm. Res., 134*, 77-107.

Patrick, M. (2007), The gas content and buoyancy of Strombolian ash plumes, *J. Volcanol. Geotherm. Res., 166*, 1-6.

Patrick, M.R., A.J.L. Harris, M. Ripepe, J. Dehn, D.A. Rothery, and S. Calvari (2007), Strombolian explosive styles and source conditions: insights from thermal (FLIR) video, *Bull. Volcanol.*, *69*, 769-784.

Platt, U., and J. Stutz (2008), Differential Optical Absorption Spectroscopy Principles and Applications, in *Physics of Earth and Space Environments*, Springer.

Rodgers, C. (2000), Inverse Methods For Atmospheric Sounding, Theory and Practice, *Series on Atmospheric, Oceanic and Planetary Physics*, vol. 2, edited by F.W. Taylor, World Scientific Publishing, Singapore, pp. 256, ISBN: 9789812813718.

Rothman, L.S., C.P. Rinsland, A. Goldman, S.T. Massie, D.P. Edwards, J.-M. Flaud, A. Perrin, C. Camy-Peyret, V. Dana, J.-Y. Mandin, J. Schroeder, A. McCann, R.R. Gamache, R.B. Wattson, K.Yoshino, K.V. Chance, K.W. Jucks, L.R. Brown, V. Nemtchinov, and P. Varanasi (1998), The HITRAN Molecular Spectroscopic Database and HAWKS (HITRAN Atmospheric Workstation), 1996 Edition, *J. Quant. Spectrosc. Radiat. Transfer, 60*, 665-710.

Rowland, S.K., A.J.L. Harris, M.J. Wooster, F. Amelung, H. Garbeil, L. Wilson, and P.L. Mouginis-Mark (2003), Volumetric Characteristics of Lava Flows from Interferometric Radar and Multispectral Satellite Data, *Bull. Volcanol.*, *65(5)*, 311-330.

Salerno, G.G., M.R. Burton, C. Oppenheimer, T. Caltabiano, D. Randazzo, N. Bruno, and V. Longo (2009a), Three-years of $SO_2$ flux measurements of Mt. Etna using an automated UV scanner array: Comparison with conventional traverses and uncertainties in flux retrieval, *J. Volcanol. Geotherm. Res., 183*, 76-83, doi:10.1016/j.jvolgeores.2009.02.013.

Salerno, G.G., M.R. Burton, C. Oppenheimer, T. Caltabiano, V.I. Tsanev, and N. Bruno (2009b), Novel retrieval of volcanic $SO_2$ abundance from ultraviolet spectra, *J. Volcanol. Geotherm. Res., 181*, 141-153, doi:10.1016/j.jvolgeores.2009.01.009.

Spampinato, L., S. Calvari, C. Oppenheimer, and E. Boschi (2011), Volcano surveillance using infrared cameras, *Earth Sci. Rev.*, *106*, 63-91, doi:10.1016/j.earscirev.2011.01.003.

Spampinato, L., S. Calvari, C. Oppenheimer, and L. Lodato (2008), Shallow magma transport for the 2002-03 Mt. Etna eruption inferred from thermal infrared surveys, *J. Volcanol. Geotherm. Res., 177*, 301-312, doi:10.1016/j.jvolgeores.2008.05.013.

Sparks, R.S.J. (2003), Dynamic of magma degassing, in *Volcanic degassing*, edited by C. Oppenheimer, D.M. Pyle, and J. Barclay, pp. 213, Geological Society, London.

Sparks, R.S.J., M.I. Bursik, S.N. Carey, J.S. Gilbert, L.S. Glaze, H. Sigurdsson, and A.W. Woods, (1997), *Volcanic plumes*, Wiley, 574 pp.

Spilliaert, N., P. Allard, N. Métrich, and A.V. Sobolev (2006), Melt inclusion record of the conditions of ascent, degassing, and extrusion of volatile-rich alkali basalt during the powerful 2002 flank eruption of Mount Etna (Italy), *J. Geophys. Res.*, *111,* (B04203), doi: 10.1029/2005JB003934.

Steffke, A.M., A.J.L. Harris, M. Burton, T. Caltabiano, and G.G. Salerno (2011), Coupled Use of COSPEC and Satellite Measurements to Define the Volumetric Balance During Effusive

Eruptions at Etna, Italy, *J. Volcanol. Geotherm. Res.*, *205*, 45-53, doi: 10.1016/j.jvolgeores.2010.06.004.

Swanson, D.A., W.A. Duffield, D.B. Jackson, and D.W. Peterson (1979), Chronological narrative of the 1969-71 Mauna Ulu eruption of Kīlauea Volcano, Hawai`I, U.S. Geol. Sur., Prof. Pap., 1056, 55.

Vergniolle, S., C. Jaupart (1986), Separated two-phase flow and basaltic eruptions. *J. Geophys. Res.*, *91*, 12842-12860.

Vergniolle, S., and M.T. Mangan (2000), Hawaiian and Strombolian eruptions, in *Encyclopedia of Volcanoes*, edited by H. Sigurdsson, B. Houghton, S.R. McNutt, H. Rymer, and J. Stix, pp. 447-461, Academic Press, San Diego, CA.

Vergniolle, S., and M. Ripepe (2008), From Strombolian explosions to fire fountains at Etna Volcano (Italy): what do we learn from acoustic measurements? in *Fluid Motions in Volcanic Conduits: A source of Seismic and Acoustic Signals*, edited by S.J. Lane and J.S. Gilbert, pp. 103-124, Geol. Soc. Spec. Publ., vol. 307, London.

Vicari, A., G. Ganci, B. Behncke, A. Cappello, M. Neri, and C. Del Negro (2011), Near-real-time forecasting of lava flow hazards during the 12-13 January 2011 Etna eruption, *Geophys. Res. Lett.*, *138*, L13317, doi: 10.1029/2011GL047545.

Wolfe, E.W., C.A. Neal, N.G. Banks, and T.J. Duggan (1988), Geologic observations and chronology of eruptive events, in *The Puu Oo eruption of Kilauea Volcano, Hawaii: Episodes 1 through 20, January 3, 1983, through June 8, 1984*, U.S. Geol. Survey Professional Paper, vol. 1463, pp. 1-98.

Wooster, M.J., R. Wright, S. Blake, D.A. Rothery (1997), Cooling mechanisms and an approximate thermal budget for the 1991-1993 Mount Etna lava, *Geophys. Res. Lett., 24,* 277-3280.

Wright, R., and L. Flynn (2004), Space-based estimate of the volcanic heat flux into the atmosphere during 2001 and 2002, *Geology, 32(3)*, 189-192.

Table 1 – Details on the INGV-CT network of monitoring cameras. (v) = vertical; (h) = horizontal. See Figure 1 for site location.

| **Location** | **Acronym** | **Kind** | **Elevation** | **Distance from Etna's summit** | **Field Of View (FOV) And range in meters** |
|---|---|---|---|---|---|
| La Montagnola | EMOT | Thermal | 2600 m a.s.l. | 3 km | 18.8° (v) - 25° (h) |
| La Montagnola | EMOV | Visible | 2600 m a.s.l. | 3 km | 3° to 47.5°(h)<br>170 to 2860 m (h) |
| Schiena dell'Asino | ESV | Visible | 1985 m a.s.l. | 4.9 km | 2.8° to 48°(h)<br>260 to 4720 m (h) |
| Milo | EMV | Visible | 770 m a.s.l. | 10.75 km | 3° to 47.5°(h)<br>592 to 9944 m (h) |
| Nicolosi | ENT | Thermal | 730 m a.s.l. | 15 km | 18° (v) - 24° (h) |
| Nicolosi | ENV | Visible | 730 m a.s.l. | 15 km | 3° to 47.5°(h)<br>785 to 13200 m (h) |
| Catania - CUAD | ECV | Visible | 35 m a.s.l. | 26.7 km | 3° to 47.5°(h)<br>1388 to 23320 m (h) |

## Figures

Figure 1. (a) Map of the SE flank of Etna (modified after Behncke et al., 2009) showing the location of the INGV-CT thermal (red circles) and visible (yellow circles) camera stations (see Table 1 for details). Blue circles indicate the position of UV-scanner stations of the FLAME network. Labels are as follows: EMOT, EMOV = thermal and visible cameras located at La Montagnola; ESV = visible camera located at Schiena dell'Asino; EMV = visible camera located at Milo; ENT, ENV = thermal and visible cameras located at Nicolosi; ECV = visible camera located at CUAD. The black triangle indicates the position of the summit craters (magnified in b), and the rectangle is the area effected by the 11-13 January 2011 eruption and represented in Figure 2. (b) Map of southern Italy, showing the position of Sicily and Mount Etna. (c) The summit craters of Mount Etna (modified after Neri et al., 2008). Labels are as follows: NEC = NE-Crater; VOR = Voragine; NW BN: NW pit of Bocca Nuova; SE BN: SE pit of Bocca Nuova; SEC: SE-Crater.

Figure 2. Photo of the 12-13 January 2011 lava flow field taken from E during an airplane survey on 13 January. The yellow dotted line marks the boundary of the lava flow field, and the red dotted line shows the SSW dispersed ash erupted during the lava fountaining episode. The red circle displays the location of the pit crater on the eastern flank of the SEC that gave rise to the 11-13 January eruptive activity, and the black dotted square shows the area framed by EMV and displayed in Figure 4. La Montagnola is the location of EMOT and EMOV cameras (~3 km from the SEC, see figure 1). Photo courtesy of Alfio Amantia.

Figure 3. Thermal images recorded from EMOT (see Figure 1). The saturated portion of the eruptive vent and lava fountain is displayed in white. On the black line below each image we give the date (dd-mm-yyyy) and UTC time (hh:mm:ss:00). Note the eastward (right) shift of the vent as apparent by comparing b and l, and which occurred between e (21:52:43) and f (22:06:02).

Figure 4. Visible images collected from EMV and giving a view from E, over a 11 km distance, of the eruption site. (a) The brightest spot represents the strombolian activity from the pit crater on the E flank of the SE Crater, the smaller spot on the left being the lava flow from the lower rim of the pit crater. (b) Strombolian activity increases, and the lava flow spreads SE. (c) Low lava fountaining starts, with a small ash plume dispersed SE (left) and lava flow extending down the upper

Valle del Bove. (d-g) Lava fountaining increases in intensity and lava flow field grows. (h) Decreasing explosive phase and declining lava output. (i) Daytime view on 13 January, showing red ash emission from the pit crater, and the inactive lava flow field in the upper Valle del Bove is clearly visible, although partially obscurred to the left by a tree. Date and time formats are as in Figure 3.

Figure 5. (a-f) View of the summit of Mt. Etna from S over a distance of ~27 km (from ECV). A horizontal scale (for the location of SEC) of 800 m is displayed in (a). (b) The ash column is forming over the lava fountaining, and lava flow is spreading E towards the Valle del Bove. (c) Both the height of the eruptive column, lava fountaining and length of the lava flows increase, and a dust cloud is forming above the lava flow front. (d) The ash column spreads both laterally (upper part) and southward, partially obscuring the lava fountaining. (e) The lava flows become brighter, and also the dust cloud from the flow front spreads laterally. (f) The lava flows expand within the Valle del Bove; the flow fronts are now hidden behind its S rim. The ash plume spreading S hides the lava fountaining. (g-i) Thermal images from Nicolosi (ENT) showing lava fountaining (white-red) and the associated ash plume (bluish to purple). The dust plume to the right is from the lava flow fronts. (j) Graph of the apparent temperature recorded by ENT and detected through the NewSaraterm software, showing the thermal signals associated with the transitional explosive phase, the lava fountain, and the final ash explosion.

Figure 6. (a) Number of explosions occurring in 15 minutes time windows during 11-12 January 2011. The grey shaded area lacks data due to clouds obscuring the summit. (b) Time evolution of active lava flow area (blue line) and lava fountain area (red line), as seen from EMV.

Figure 7. (a) Long-term variations in the 7-point-running mean $SO_2$ flux (red line; primary y-axis) and discrete HCl and HF flux measurements (green and light blue lines, respectively; secondary y-axis). Note that, to plot HF flux on the y-axis, we have multiplied it by five. (b) Daily-averaged $SO_2$ flux measured by the Flame network between 2 and 19 January 2011, together with the HCl (green starts) and HF (light blue triangles) fluxes measured on 11 and 14 January. (c) Magnified time-window showing the daytime $SO_2$ flux measured between 10 and 14 January 2011. Dotted-blue lines indicate the onset of the strombolian (str) and lava fountain (lf) activity.

Figure 8. Graph of the height (a), width (b) and area (c) of the lava fountains calculated from the images of EMV (Milo) and EMOT (La Montagnola) against time during the fountaining episode of 12-13 January 2011.

Figure 9. Photo (a) and corresponding thermal image (b) of the lava flow field emplaced in the Valle del Bove on 12-13 January 2011, taken from SE. Both images show that the lava flow field is cooling. The high temperature areas of the lava flow field relate to the front widening on Valle del Bove floor and to still moving lava due to channel drianage. Photograph in (a) is courtesy of Stefano Branca.

Figure 10. Power flux extracted from SEVIRI data showing the trends associated with lava emission, plume obscuration, saturation, and cooling. During the effusive phase power flux was converted to TADR using model parameters given [see *Gouhier et al*., 2011]. In addition the cooling curve was used to estimate the total volume of erupted lava, allowing us to reconstruct the TADR curve as given at the right. For the TADR curve, TADRs calculated using unsaturated, cloud-free data are given by dark tones, and the "missing" volume obtained from the cooling curve is given by the light tones.

Figure 11. Number of explosions and daytime $SO_2$ flux recorded on 12 January 2011.

Figure 12. Photo taken from E during a 14 January 2011 overflight showing the depression on the East flank of the SE-Crater (pit crater) which was the source of explosive and effusive activity on 11-13 January 2011. Volcanic ash dispersal covering the snow towards S (left in the picture) does not cover the summit of the SE-Crater, thus showing that this crater did not produce any explosive activity during the eruptive episode. Note the two lava flows extending from the depression on the East flank of the SEC towards the Valle del Bove, which were emplaced during the night of 12-13 January. The two rootless flows produced by the remobilization of tephra have been marked using a yellow dotted line. Photo courtesy of Alfio Amantia.

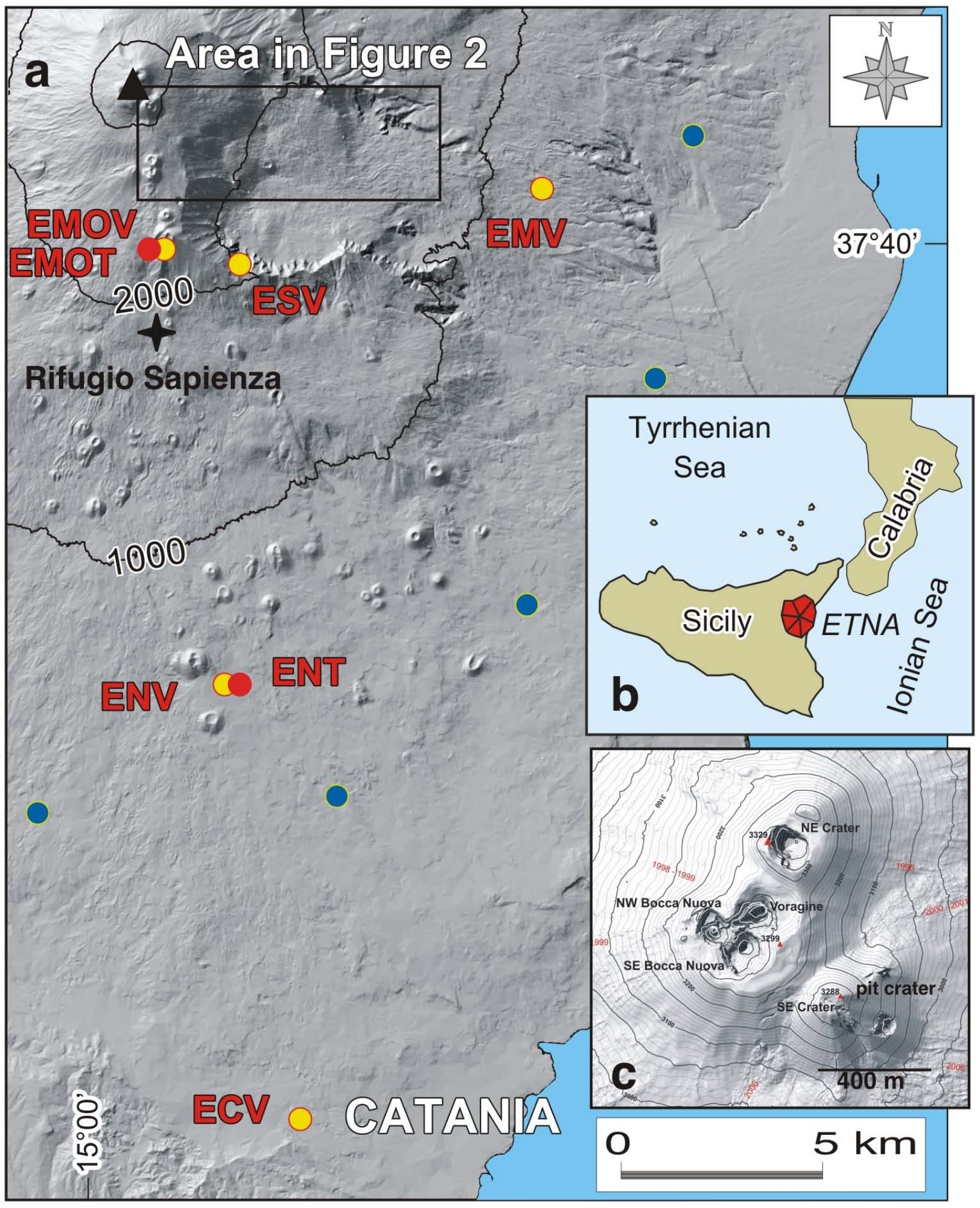
a
Area in Figure 2
N
EMOV
EMOT
EMV
ESV
2000
Rifugio Sapienza
37°40'
1000
ENV
ENT
ECV
CATANIA
15°00'
Tyrrhenian Sea
Calabria
Sicily
ETNA
Ionian Sea
b
NE Crater
3329
1998
1999
NW Bocca Nuova
Voragine
3299
SE Bocca Nuova
3288
pit crater
SE Crater
3100
3200
2000
2001
2006
c
400 m
0
5 km

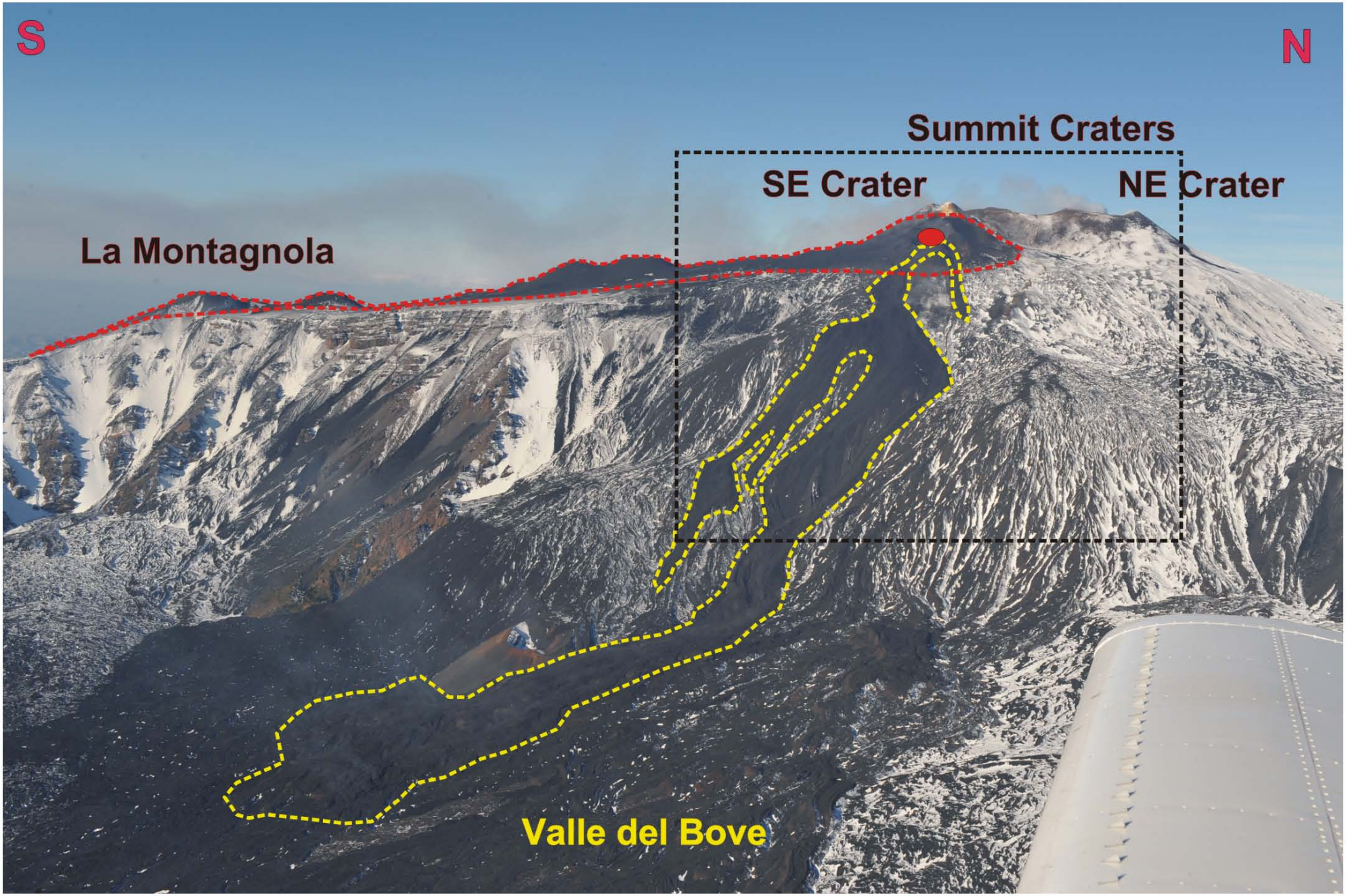
S
N
Summit Craters
SE Crater
NE Crater
La Montagnola
Valle del Bove

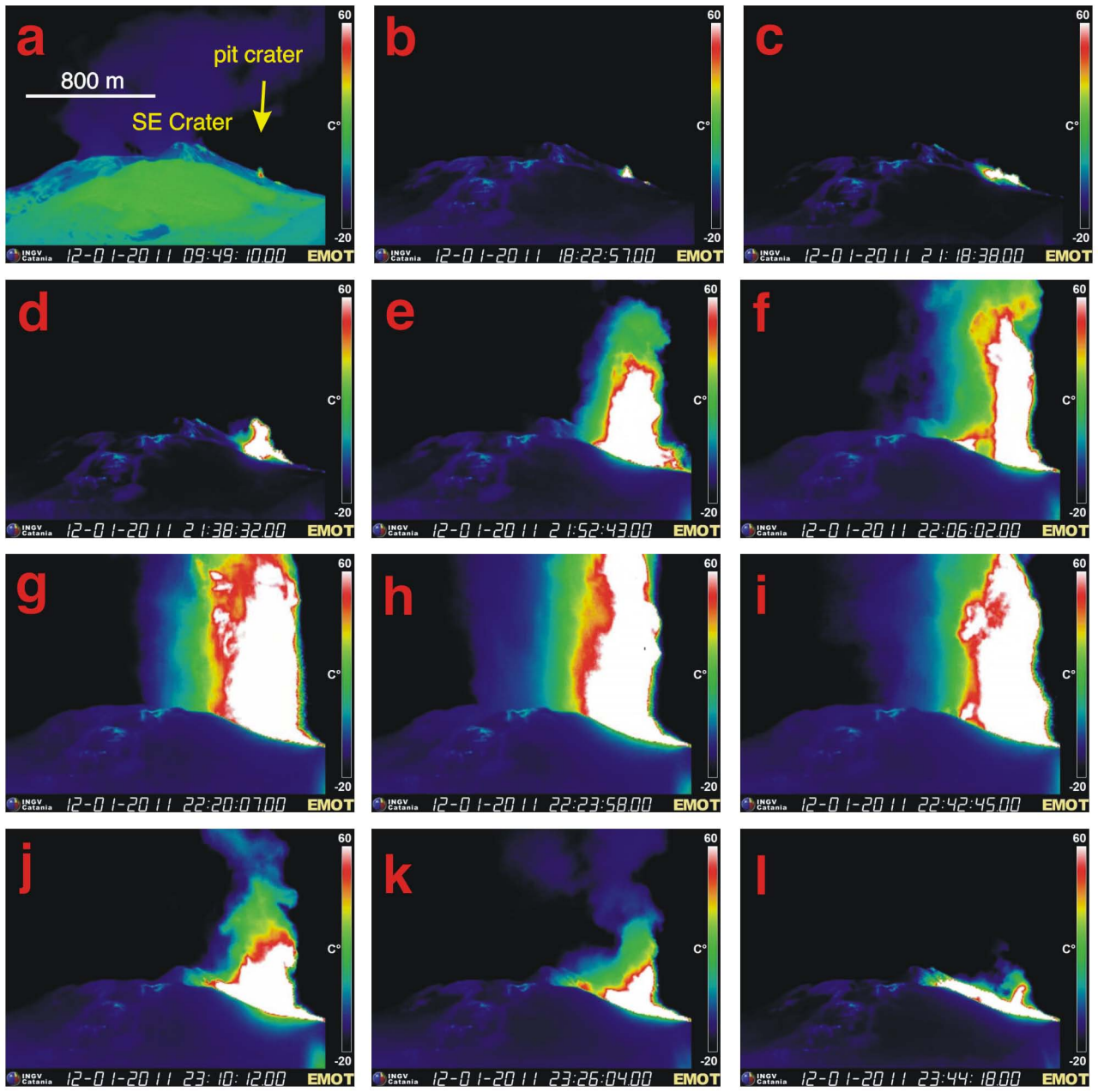
a
pit crater
800 m
SE Crater
60
C°
-20
INGV Catania
12-01-2011 09:49:10.00
EMOT
b
12-01-2011 18:22:57.00
c
12-01-2011 21:18:38.00
d
12-01-2011 21:38:32.00
e
12-01-2011 21:52:43.00
f
12-01-2011 22:06:02.00
g
12-01-2011 22:20:07.00
h
12-01-2011 22:23:58.00
i
12-01-2011 22:42:45.00
j
12-01-2011 23:10:12.00
k
12-01-2011 23:26:04.00
l
12-01-2011 23:44:18.00

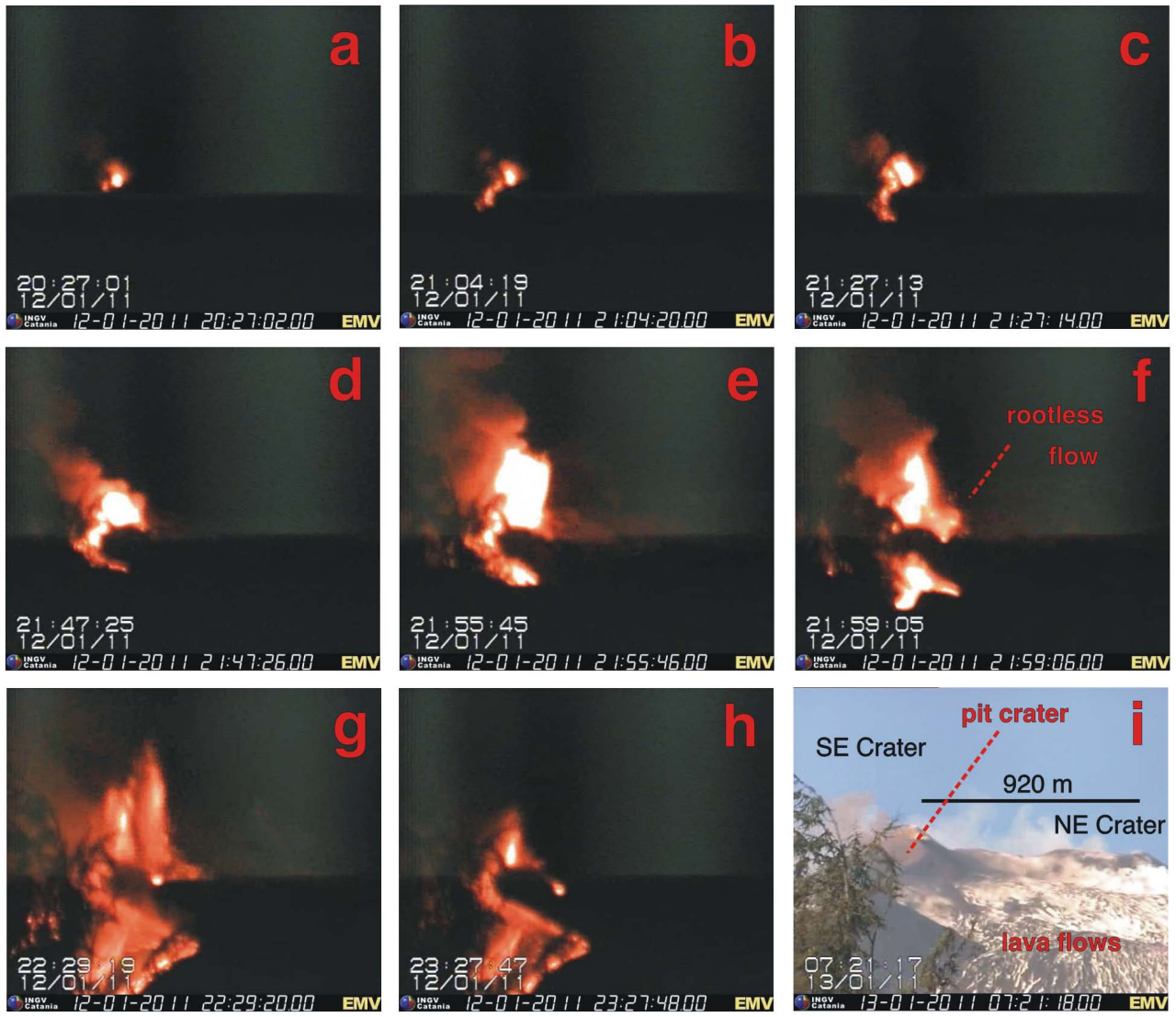
a
20:27:01
12/01/11
12-01-2011 20:27:02.00
EMV
b
21:04:19
12/01/11
12-01-2011 21:04:20.00
EMV
c
21:27:13
12/01/11
12-01-2011 21:27:14.00
EMV
d
21:47:25
12/01/11
12-01-2011 21:47:26.00
EMV
e
21:55:45
12/01/11
12-01-2011 21:55:46.00
EMV
f
rootless
flow
21:59:05
12/01/11
12-01-2011 21:59:06.00
EMV
g
22:29:19
12/01/11
12-01-2011 22:29:20.00
EMV
h
23:27:47
12/01/11
12-01-2011 23:27:48.00
EMV
i
pit crater
SE Crater
920 m
NE Crater
lava flows
07:21:17
13/01/11
13-01-2011 07:21:18.00
EMV

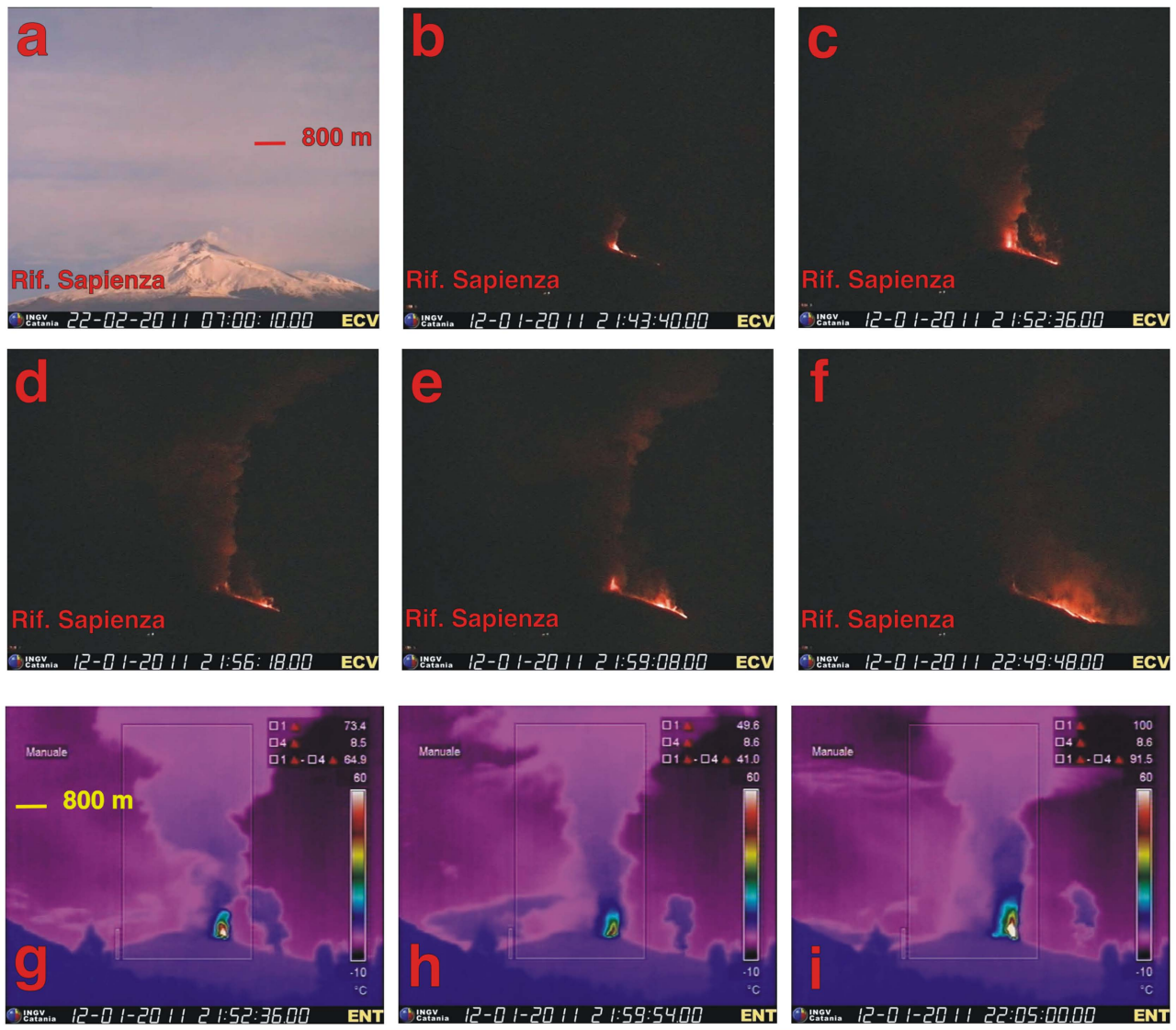
a
800 m
Rif. Sapienza
22-02-2011 07:00:10.00 ECV
b
Rif. Sapienza
12-01-2011 21:43:40.00 ECV
c
Rif. Sapienza
12-01-2011 21:52:36.00 ECV
d
Rif. Sapienza
12-01-2011 21:56:18.00 ECV
e
Rif. Sapienza
12-01-2011 21:59:08.00 ECV
f
Rif. Sapienza
12-01-2011 22:49:48.00 ECV
g
Manuale
800 m
12-01-2011 21:52:36.00 ENT
h
Manuale
12-01-2011 21:59:54.00 ENT
i
Manuale
12-01-2011 22:05:00.00 ENT
j
fire fountains
transitional
ash expl.
TEMPERATURE (°C)
TIME and DATE

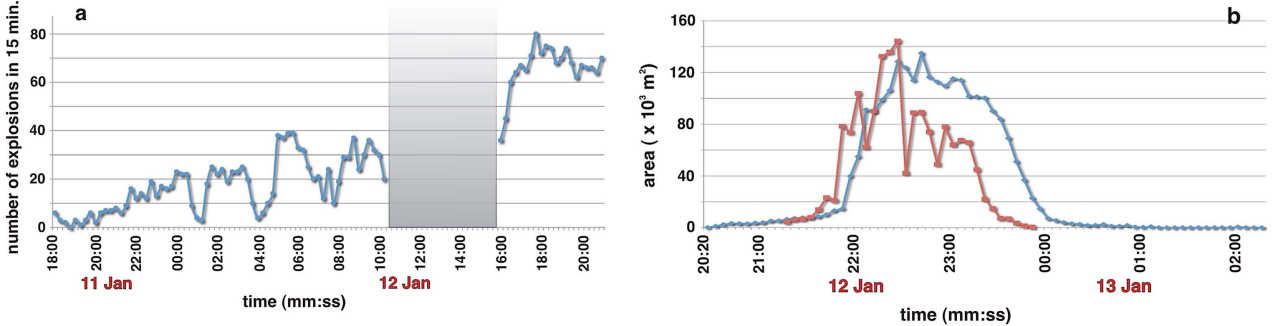
a
number of explosions in 15 min.
0
20
40
60
80
18:00
20:00
22:00
00:00
02:00
04:00
06:00
08:00
10:00
12:00
14:00
16:00
18:00
20:00
11 Jan
12 Jan
time (mm:ss)
b
area ( x 10³ m²)
0
40
80
120
160
20:20
21:00
22:00
23:00
00:00
01:00
02:00
12 Jan
13 Jan
time (mm:ss)

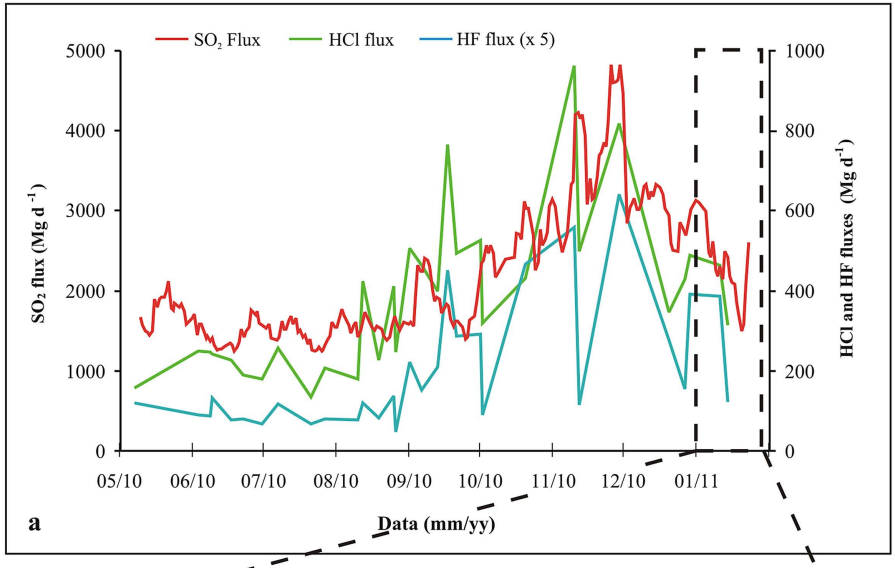
SO2 Flux
HCl flux
HF flux (x 5)
SO2 flux (Mg d-1)
HCl and HF fluxes (Mg d-1)
05/10
06/10
07/10
08/10
09/10
10/10
11/10
12/10
01/11
Data (mm/yy)
a

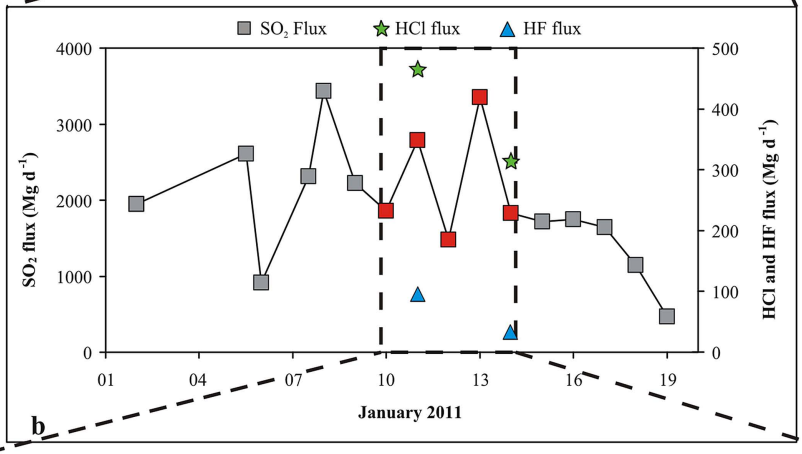
SO2 Flux
HCl flux
HF flux
SO2 flux (Mg d-1)
HCl and HF flux (Mg d-1)
January 2011
b

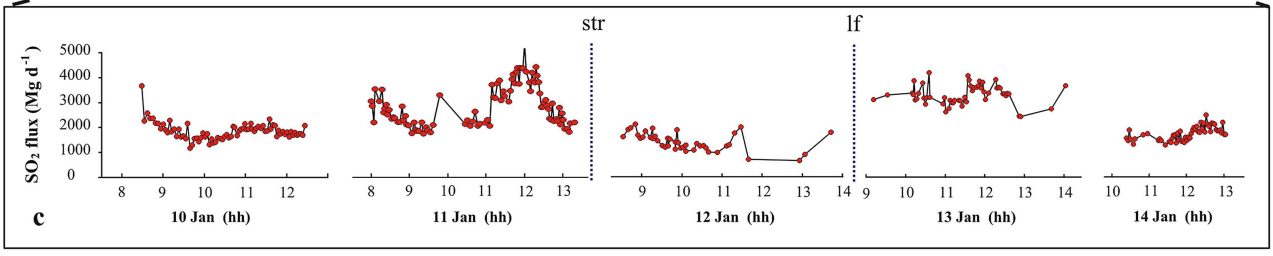
str
lf
SO2 flux (Mg d-1)
10 Jan (hh)
11 Jan (hh)
12 Jan (hh)
13 Jan (hh)
14 Jan (hh)
c

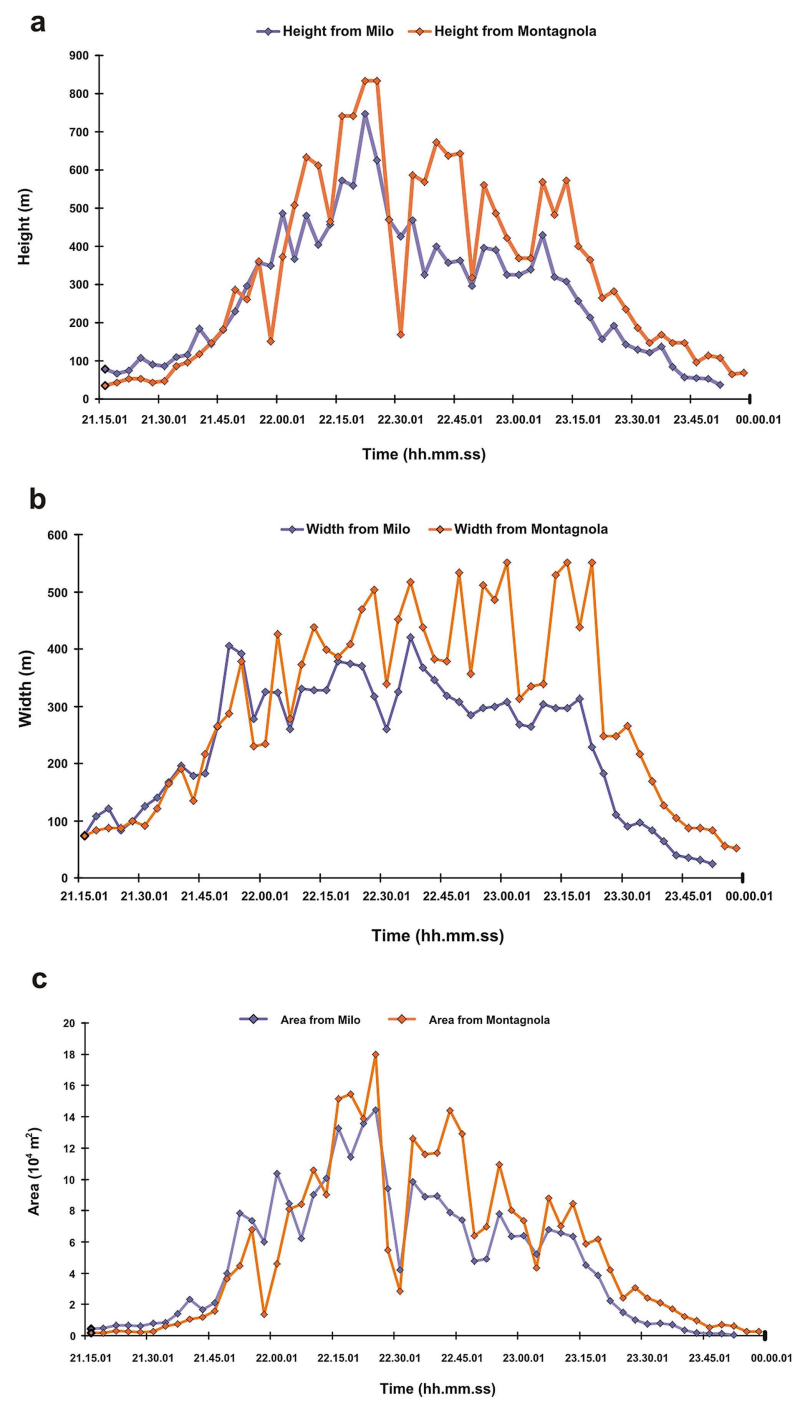
a
Height from Milo
Height from Montagnola
Height (m)
900
800
700
600
500
400
300
200
100
0
21.15.01
21.30.01
21.45.01
22.00.01
22.15.01
22.30.01
22.45.01
23.00.01
23.15.01
23.30.01
23.45.01
00.00.01
Time (hh.mm.ss)
b
Width from Milo
Width from Montagnola
Width (m)
600
500
400
300
200
100
0
21.15.01
21.30.01
21.45.01
22.00.01
22.15.01
22.30.01
22.45.01
23.00.01
23.15.01
23.30.01
23.45.01
00.00.01
Time (hh.mm.ss)
c
Area from Milo
Area from Montagnola
Area ($10^4$ $m^2$)
20
18
16
14
12
10
8
6
4
2
0
21.15.01
21.30.01
21.45.01
22.00.01
22.15.01
22.30.01
22.45.01
23.00.01
23.15.01
23.30.01
23.45.01
00.00.01
Time (hh.mm.ss)

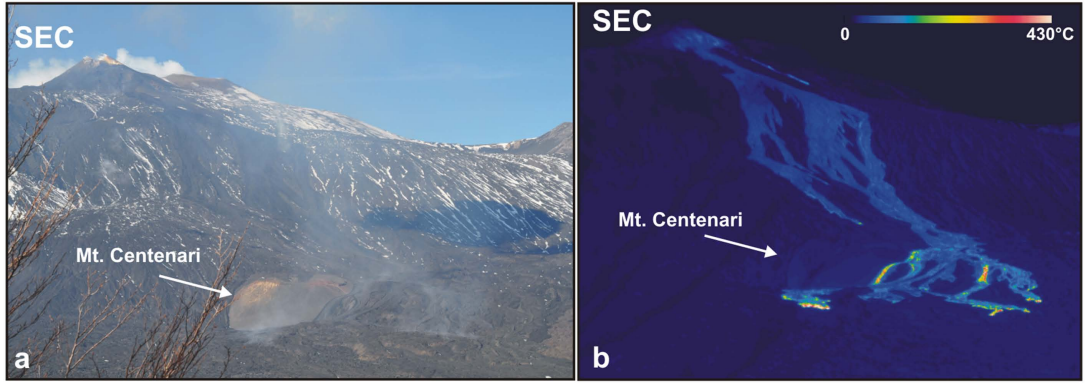
SEC
Mt. Centenari
a
SEC
0
430°C
Mt. Centenari
b

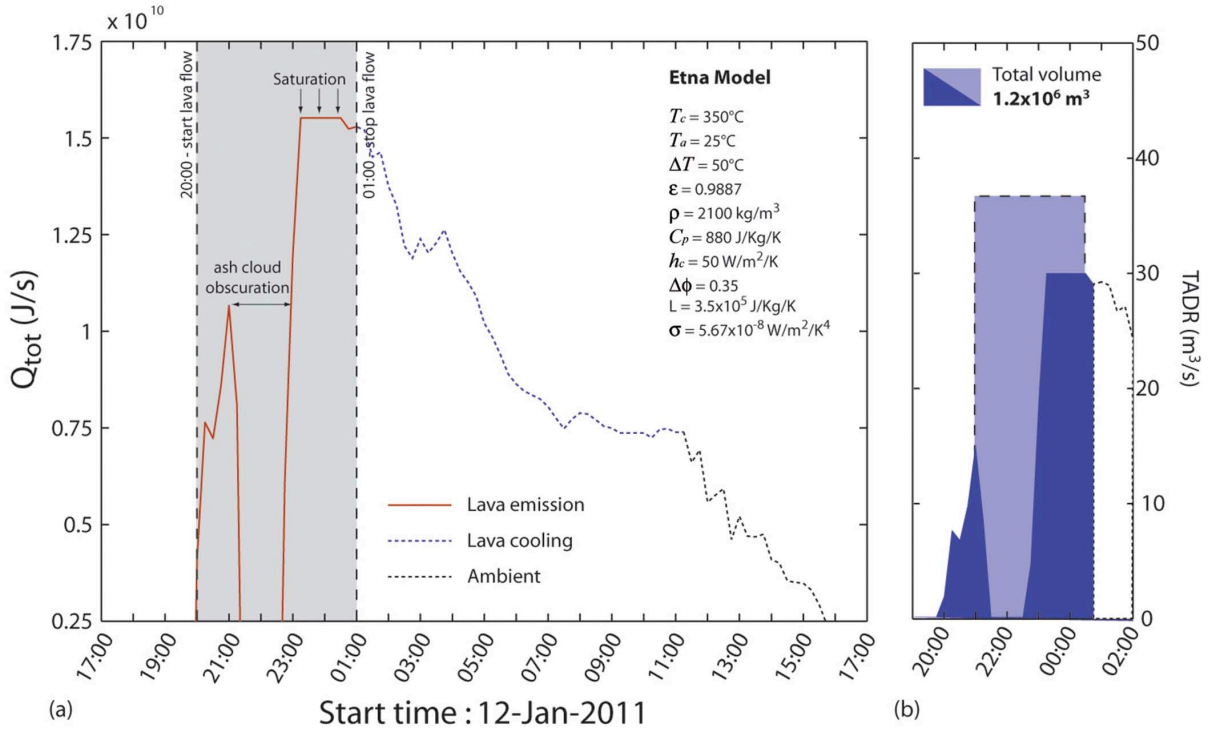
x 10^10
1.75
1.5
1.25
1
0.75
0.5
0.25
Qtot (J/s)
20:00 - start lava flow
01:00 - stop lava flow
Saturation
ash cloud obscuration
Etna Model
Tc = 350°C
Ta = 25°C
ΔT = 50°C
ε = 0.9887
ρ = 2100 kg/m3
Cp = 880 J/Kg/K
hc = 50 W/m2/K
Δϕ = 0.35
L = 3.5x10^5 J/Kg/K
σ = 5.67x10^-8 W/m2/K4
Lava emission
Lava cooling
Ambient
17:00
19:00
21:00
23:00
01:00
03:00
05:00
07:00
09:00
11:00
13:00
15:00
17:00
(a)
Start time : 12-Jan-2011
Total volume
1.2x10^6 m3
50
40
30
20
10
0
TADR (m3/s)
20:00
22:00
00:00
02:00
(b)

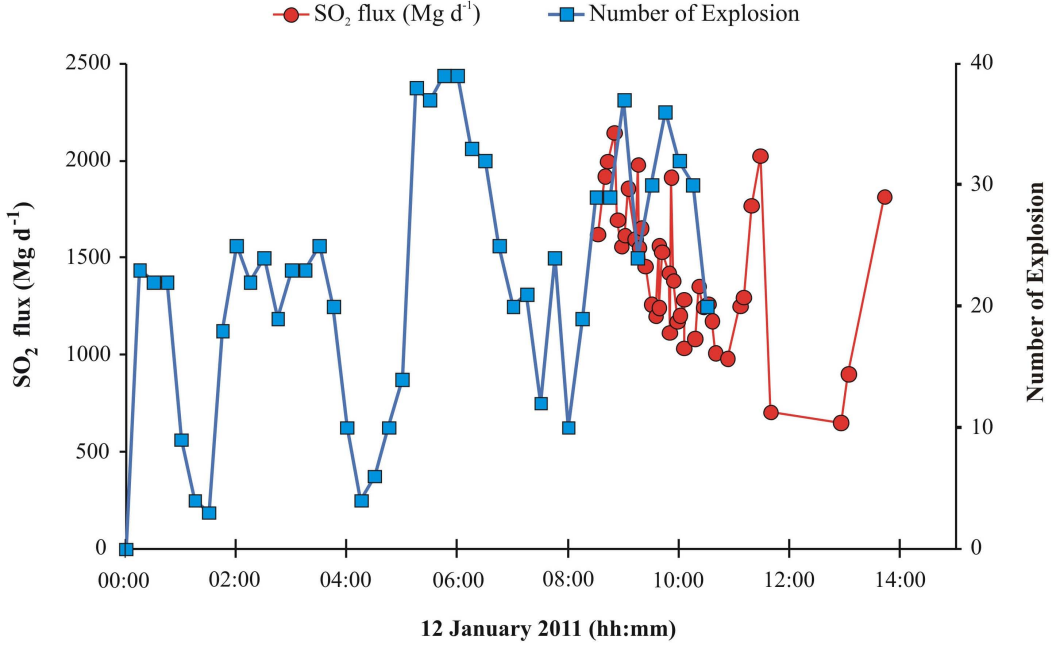
SO2 flux (Mg d-1)
Number of Explosion
2500
2000
1500
1000
500
0
40
30
20
10
0
00:00
02:00
04:00
06:00
08:00
10:00
12:00
14:00
12 January 2011 (hh:mm)

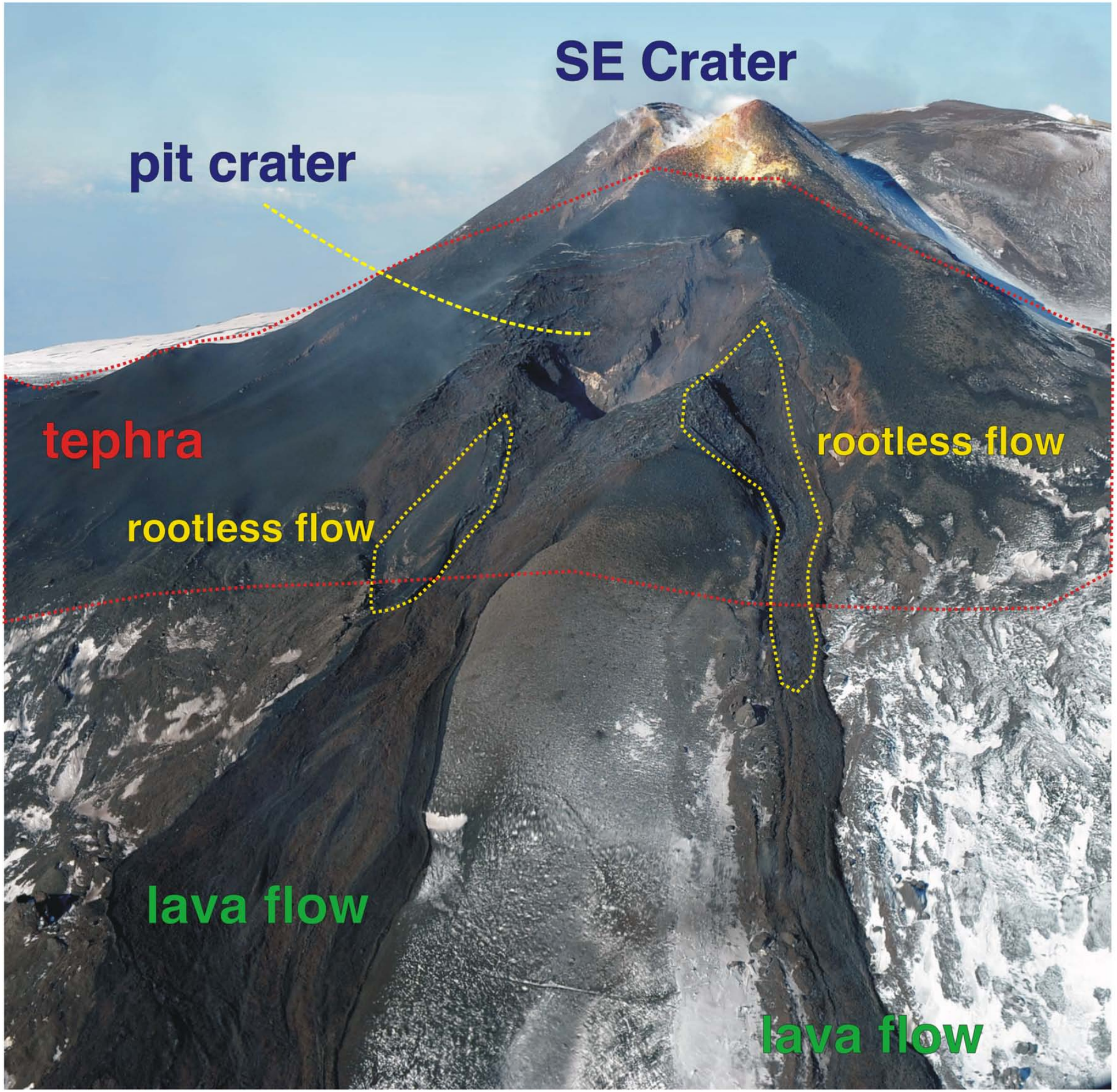
SE Crater
pit crater
tephra
rootless flow
rootless flow
lava flow
lava flow